Analytical study for double-layer geosynthetic reinforced load transfer platform on column improved soft soil

Balaka Ghosh[1], Behzad Fatahi[2*], Hadi Khabbaz[3], and Jian-Hua Yin[4]

[1]PhD Candidate (MEng, BEng), School of Civil and Environmental Engineering, University of Technology Sydney (UTS), Sydney, Australia, Email: balaka.ghosh@uts.edu.au

[2]Associate Professor of Geotechnical Engineering (PhD, MEng, BEng, CPEng, NPER), School of Civil and Environmental Engineering, University of Technology Sydney (UTS), Sydney, Australia, Email: behzad.fatahi@uts.edu.au

[3]Associate Professor of Geotechnical Engineering, School of Civil and Environmental Engineering, University of Technology Sydney (UTS), Sydney, Australia, Email: hadi.khabbaz@uts.edu.au

[4]Chair Professor of Soil Mechanics, The Department of Civil and Environmental, The Hong Kong Polytechnic University, Hung Hom, Kowloon, Hong Kong, China, Email: jian-hua.yin@polyu.edu.hk

*Corresponding Author, School of Civil and Environmental Engineering
Faculty of Engineering and Information Technology
University of Technology Sydney (UTS)
City Campus PO Box 123 Broadway NSW 2007
T (+61) (2) 95147883 F (+61) (2) 95142633 M 0413573481
Email: behzad.fatahi@uts.edu.au

Analytical study for double-layer geosynthetic reinforced load transfer platform on column improved soft soil

Balaka Ghosh[1], Behzad Fatahi[2*], Hadi Khabbaz[3], and Jian-Hua Yin[4]

ABSTRACT

The objective of this study is to propose a reasonably accurate mechanical model for double-layer geosynthetic reinforced load transfer platform (LTP) on column reinforced soft soil which can be used by practicing engineers. The developed model is very useful to study the behaviour of LTP resting on soft soil improved with conventional columns such as concrete columns, piles, and deep soil mixing columns. The negligible tensile strength of granular material in LTP, bending and shear deformations of LTP, compressibility and shearing of soft soil have been incorporated in the model. Furthermore, the results from the proposed model simulating the soft soil as Kerr foundation model are compared to the corresponding solutions when the soft soil is idealised by Winkler and Pasternak foundation models. It is observed from the comparison that the presented model can be used as a tool for a better prediction of the LTP behaviour with multi layers of geosynthetics, in comparison with the situation that soft soil is modelled by Winkler and Pasternak foundations. Furthermore, parametric studies show that as the column spacing increases, the maximum deflection of LTP and normalised tension in the geosynthetics also increase. Whereas, the maximum deflection of LTP and normalised tension in the geosynthetics decrease with increasing LTP thickness, stiffness of subsoil, and stiffness of geosynthetic reinforcement. In addition, it is observed that the use of one stronger geosynthetic layer (e.g. 1×2000 kN/m) with the equivalent stiffness of two geosynthetic layers (e.g. 2×1000 kN/m) does not result in the same settlement of LTP and the tension of the geosynthetic reinforcement when compared to two weaker geosynthetic layers.

Keywords: Geosynthetics; Soil-structure interaction; Timoshenko beam; Load transfer platform; Multilayer; Soft soil

1. Introduction

Insufficient bearing capacity and excessive settlement are very common and severe issues of soft soils when heavy superstructures are constructed on the top of these soils (Parsa-Pajouh et al., 2016). Thus, in combination with cautious field observations and laboratory tests, the use of ground improvement techniques using rigid (e.g. concrete injected columns, jet grouted columns, and piles) or semi-rigid inclusions (e.g. deep soil mixing columns and lime-cement columns) has grown substantially over the last two decades (Bergado et al., 1999; Han et al., 2004). Load transfer platform (LTP), a layer of sand or gravel consisting of geosynthetic layers, is commonly placed over the columns (e.g. concrete injected columns, or piles) used for ground improvement to facilitate the load transfer from the superstructures to the columns (Russell and Pierpoint, 1997; Han and Gabr, 2002; Kempfert et al., 2004).

Application of a load transfer platform resting on column improved soft soil is very common, particularly when highway embankments are built on improved ground. To analyse the column supported embankments, several analytical models have been proposed in the literature. Van Eekelen et al. (2013) summarised and classified them as (a) frictional models (Terzaghi, 1943; McKelvey, 1994; Russell and Pierpoint, 1997; Naughton, 2007; McGuire et al., 2012), (b) rigid arch models (Carlsson, 1987; Rogbeck et al., 1998; Svanø et al.; 2000; Van Eekelen et al., 2003), (c) models using mechanical elements (Deb, 2010; Filz et al.; 2012; Zhang et al., 2012a, b; Deb and Mohapatra, 2013) and (d) limit-state equilibrium models (Marston and Anderson, 1913; Hewlett and Randolph, 1988; Jones et al., 1990; Zaeske, 2001). British design guidelines BS8006 (2010), discussed by Van Eekelen et al. (2011), adopted the empirical model proposed by Jones et al. (1990) to study the geosynthetic reinforced column supported embankments. Zaeske's model (2001) latter was adopted in the German design guidelines EBGEO (2010). Van Eekelen et al. (2013) proposed a new limit-state equilibrium model for piled embankments which is an extension of the model proposed by Hewlett and Randolph (1988) and EBGEO (2010). Several other researchers compared the results of existing analytical models with field or laboratory measurements (Chen et al., 2008; Chen et al., 2010; Briançon and Simon, 2012; Girout et al., 2016). Chen et al. (2008) conducted experiments both with and without geosynthetics and compared the results of their experiments with existing analytical models, namely Terzaghi (1943) and Low et al. (1994) and the original 2D equation of Marston and Anderson (1913). Zaeske (2001), Heitz (2006), and Farag (2008) compared the results of their laboratory model tests with their predictions from the calculations. Results of a predictive model to capture membrane behaviour of the geosynthetic reinforcement based on the results of twelve model tests have been reported by Van Eekelen et al. (2012a, b). Several other studies have been conducted using two dimensional numerical models of geosynthetic reinforced column supported embankment structures adopting the finite element method (FEM) and finite difference method (FDM) (Han et al., 2007; Huang et al., 2009; Huang and Han, 2010; Yapage and Liyanapathirana, 2014). Furthermore, the predictions adopting full-width model were compared with unit cell model in numerical simulations by Bhasi and Rajagopal (2015), Khabbazian et al. (2015), and Yu and Bathurst (2017). Collin et al. (2005) proposed a mechanical model of multiple layers of low strength geogrids within the LTP based on the concept of "beam" theory. But, the interrelationship between the embankment settlement and strain in the geosynthetics was ignored in that study. However, application of a load transfer platform is not limited to the column supported embankments. Load transfer platform is widely used for heavy superstructures such as fuel tanks and silos. The practical designs of LTP demand the simple yet accurate modelling of (i) the mechanical behaviour of the LTP, (ii) the mechanical behaviour of the underneath soft soil, and (iii) the interaction mechanism between the LTP and the soft soil.

While physically close and mathematically simple idealisations of the mechanical behaviour of the geosynthetic reinforced granular fill or LTP can be established adopting Timoshenko (Yin, 2000a, b; Shukla and Yin, 2003; Zhao et al., 2016) or the Euler-Bernoulli beam theories (Maheshwari et al., 2004; Maheshwari and Viladkar, 2009; Zhang et al., 2012a, b) or even the Pasternak shear layer theory (Yin, 1997a, b; Deb et al., 2007; Deb, 2010), the characteristics that represent the mechanical behaviour of the soft soil and its interaction with the granular layer are difficult to model. Since in reality, the soft soil is heterogeneous, anisotropic and nonlinear in load-displacement response, the simple springs cannot simulate the soil response accurately. It should be noted that the most commonly used mechanical model to simulate the soil is the one developed by Winkler (1867). Although, the model proposed by Van Eekelen et al. (2013) can be applicable for both full and partial arching which results in a better representation of the arching measured in the experiments than the other existing models such as EBGEO (2010), BS8006 (2010), especially when the embankment is relatively thin, Van Eekelen et al. (2013) modelled the subsoil as an elastic spring with constant modulus of subgrade reaction which is comparable to linear Winkler's springs. Winkler's idealisation symbolises the soil medium as a series of identical but mutually independent, closely spaced, linearly elastic spring elements. Since according to the Winkler hypothesis, there is no interaction between adjacent springs, this model cannot account for the dispersion of the load with depth and distance from the loading area. However, it is a common phenomenon that the surface deflections occur not only immediately under the loaded region but also within certain limited regions beyond the loaded area. Therefore, Winkler's model has the inability to take into account the continuity or shear strength of the soil. Hence, compressibility of the soil was considered in the model proposed by Van Eekelen et al. (2013) while shear action in the soil was ignored. To overcome the weaknesses of the Winkler's model (i.e. to achieve some degree of interaction between the individual spring elements), some modified foundation models have been suggested in the literature. In these modified models, a second parameter was introduced to Winkler foundation to eliminate the discontinuous behaviour of soil by providing continuity through interaction between the individual spring elements with some structural elements (Filonenko-Borodich, 1940; Hetényi, 1946; Pasternak, 1954). To further improve the two-parameter foundation models, the third soil parameter was introduced, leading to the so-called "three-parameter" foundation model. Among several three-parameter foundation models, the foundation model proposed by Kerr (1965) is of particular interest since it geneses from the well-known Pasternak foundation model for which several applications and solutions have been already available in the literature. Kerr foundation model consists of two spring layers, with varied spring constants, interconnected by a shear layer. Furthermore, Kerr concluded that for different types of foundation materials (e.g. soil and foam), the Winkler foundation model cannot realistically predict the interaction mechanisms between the beams and the contacting soil medium. Therefore, the most important task for practicing engineers is to simulate soft soil, which demands simple modelling but provides an accurate response of the soft soil.

Mechanical behaviour of the geosynthetic reinforced granular fill or LTP can be theoretically established by adopting the Pasternak shear layer theory (Yin, 1997a, b; Deb et al., 2007; Deb, 2010), the Euler-Bernoulli beam theory (Maheshwari et al. 2004; Maheshwari and Viladkar, 2009; Zhang et al., 2012a, b), and the Timoshenko beam theory (Yin, 2000a, b; Shukla and Yin, 2003; Zhao et al., 2016). According to Pasternak theory, the cross-section of the LTP does not rotate and therefore, the granular layer experiences transverse shear deformation only. Thus, bending deformation of the granular layer was ignored in the developed models (Yin, 1997a, b; Deb et al., 2007; Deb, 2010). For application of the Euler-Bernoulli theory in geosynthetic reinforced soil (Maheshwari et al. 2004; Maheshwari and Viladkar, 2009; Zhang et al., 2012a, b), by considering the plane sections remain plane and perpendicular to the neutral axis after deformation, the shear deformation of a geosynthetic reinforced soil was ignored. However, after deformation of beams with the small length - to depth ratio, the cross section of the beam is still not be perpendicular to the neutral axis. To overcome the shortcomings of Euler-Bernoulli and Pasternak theories, the well-known Timoshenko (1921) beam can be adopted to simulate the LTP (Yin, 2000a, b). Yin (2000a, b) idealised the soft soil, the granular layer, and the geosynthetics by linear Winkler springs, Timoshenko beam, and a rough membrane, respectively. Based on the Timoshenko (1921) beam assumption, Yin's model considers the shear and the flexural deformations of the granular layer since the rotation between the cross section and the bending line of the beam is acceptable. However, the model considered a linear behaviour for soft soil, and the infinite tensile stiffness for the granular fill materials was assumed while column supports were not considered. Zhao et al. (2016) proposed a new dual beam model for a geosynthetic-reinforced granular fill with an upper pavement. Zhao et al. (2016) modelled the upper pavement by an Euler-Bernoulli beam, while the geosynthetic reinforced granular fill was simulated by a reinforced Timoshenko beam. The explicit derivation process for the behaviour of this dual beam-foundation system was presented in this study and an exact solution was suggested. However, effects of columns and negligible tensile strength of soil were not considered in that study. When the granular material in LTP is dense to very dense (relative density greater ≥ 65%) due to the compaction process, idealisation of LTP as Timoshenko beam is more appropriate (Shukla and Yin, 2003). Indeed, the total settlement of LTP can occur due to the beam bending mechanism as well as the shear action, similar to the case of a reinforced concrete beam. After a few years of operation, LTP will become stiffer and behave like a concrete beam, deforming in shear as well as in bending. Hence, the settlement analysis of LTP in the construction stage or short time after may be conducted using the existing models (Deb, 2010; Van Eekelen et al. 2013), but the model proposed in this paper can be more suitable for the latter stages of LTP life as well as construction stage or short time after construction (by assuming lower shear or bending stiffness of LTP).

Most of the analytical and numerical studies related to geosynthetic reinforced granular layer on soft soil have been conducted for the single layer geosynthetic reinforced soil system (Yin, 1997a, b; Maheshwari et al., 2004; Huang and Han, 2009; Zhao et al., 2016), while very limited number of studies have addressed multilayer geosynthetic reinforced arrangement (Nogami and Yong, 2003; Liu and Rowe, 2015; Van Eekelen et al., 2015; Borges and Gonçalves, 2016). Nogami and Yong (2003) proposed a mechanical model for a multilayer geosynthetic reinforced soil subjected to structural loading. Nogami and Yong (2003) considered each soil layer by a system of an infinite number of closely spaced one-dimensional columns connected with horizontal springs. Governing differential equations were solved iteratively by the finite difference method. Therefore, the present study is an attempt to suggest a generalised model that provides a closed-form solution to estimate the behaviour of multilayer reinforced granular fill.

The key purpose of this paper is to develop an accurate analytical model to predict behaviour of LTP on column reinforced soft soil by idealising the physical modelling of the LTP on the soil media as “membrane reinforced Timoshenko beam” on Kerr foundation. The analytical model developed in this study can be applied by practicing engineers to predict the deflection of the LTP and mobilised tension in the geosynthetic reinforcement. Then, an analytical solution for the governing differential equation is proposed. The suitability of the Kerr foundation model for engineering calculations of LTP are evaluated while LTP is subjected to symmetric loading. To solve the governing differential equations, the supports of column in the reinforced soft soil is counted in by considering the reaction force in the column locations. To validate the proposed model, the results from the proposed model simulating the soft soil as the Kerr foundation model are compared to the corresponding solutions when the soft soil is idealised by Winkler and Pasternak foundations. Similar approach to validate the analytical model was taken by several other researchers available in the literature (Maheshwari and Viladkar, 2009; Zhang et al., 2012b; Lei et al., 2016). Parametric studies are also carried out to assess the overall behaviour of the multilayer geosynthetic reinforced granular layer as well as that of the single layer geosynthetic reinforced granular layer.

2. Formulation of the problem

The proposed mechanical model that idealises the mechanistic behaviour of a load transfer platform (LTP) on column improved soft soil in plane strain condition is presented in Fig. 1a. The free body diagrams of the small segments in LTP (i.e. element A) and shear layer (i.e. element B) of length dx are shown in Figs. 1b−c, respectively. In this study, double layers of geosynthetic reinforcement embedded within compacted granular layers are considered. The geosynthetic reinforcement is modelled as a rough elastic membrane, placed inside the Timoshenko beam representing the granular fill materials. Thus, the combined representation of the geosynthetic-reinforced granular layer is a structural element named as "membrane-reinforced Timoshenko beam". Columns and soft soil are idealised by Winkler springs and Kerr foundation model, respectively. It is implicit here that granular fill material in the load transfer platform (LTP) has insignificant tensile strength compared to compressive strength, so similar to a concrete beam, tension cracks are expected to spread from the tension face (bottom edge of LTP) in the direction of the neutral axis in the span. In contrast, since the granular layer is continuous over the column positions, the direction of the bending moment changes adjacent to the columns. Accordingly, tension cracks are produced at the top edge of the granular layer and spread towards the neutral axis. A typical profile of deflection of the LTP assumed for the analytical development is shown in Fig. 2a. After cracking, it may be presumed that plane sections continue to be plane, but as the load increases, these cracks spread towards the neutral axis, and then the neutral axis starts to change its position depending on tension cracks propagation. It is assumed here that the flexural cracks are developed vertically. Since some parts of the granular layer are cracked, the soil in those fractured zones cannot sustain tensile stresses and becomes weaker. Therefore, geosynthetic reinforcement is embedded to strengthen the granular fill. Similar approach (i.e. cracked load transfer platform) was considered previously by Ghosh et al. (2016) while load transfer platform was analysed on Winkler foundation considering the non-linear behaviour of soft soils. For the sake of obtaining an analytical solution and following one of the basic assumptions used for flexural design of reinforced concrete beams, it is presumed that the geosynthetic reinforcement is attached to the granular material, thus it is reasonable to assume that the tensile and compressive forces mobilised in LTP are carried by geosynthetic reinforcement and granular material, respectively. This means the strain in the geosynthetic reinforcement is equal to the strain in the granular fill at the same level. It should be noted that by making this simplifying assumption, possible gap or slip between the geosynthetics and the granular fill materials is ignored. A similar assumption was adopted by several other researchers to study the mechanical behavior of LTP (Yin 2000a, b; Shukla and Yin, 2003). Hence, section properties of a cracked LTP should be adopted for flexural design. Since the initiation of the tension cracks and their propagation are varied in different locations, the design of LTP would be more accurate if different cross section properties in different locations of LTP are considered, depending on the locations of the tension cracks. Considering the position of the tension cracks, the loaded LTP is divided into two sections, as shown in Fig. 2a. Region I (when $-r \leq x \leq +r$) where tension cracks in the LTP appear from the bottom edge; which means the bottom of LTP is under tension (sagging moment). In contrast, in Region II (when $\pm r \leq x \leq \pm s/2$), tension cracks in the LTP develop from the top edge (hogging moment). Figs. 2b−c illustrate the effective cross sections of the LTP in Regions I and II, respectively. The cracked transformed section to carry out the flexural analysis is attained by substituting the area of geosynthetic reinforcement with an equivalent area of granular fill material equal to nA_r, where n $\left(n = E_r/E_g\right)$ is the modular ratio with the elastic modulus of geosynthetic reinforcement (E_r) and granular fill material $\left(E_g\right)$ and A_r is the cross sectional area of geosynthetic reinforcement. To analyse the response of LTP, the neutral axis is located first, positioned at a distance (h_s) from the compression end of LTP in the sagging bending moment region which is indicated in Fig. 2b. The first moment of the compression area in the LTP (A_s) above the neutral axis with respect to neutral axis must be equal that of the tension area in the transformed geosynthetic layer (nA_r^b) under the neutral axis; that is $A_s h_s/2 = nA_r^b(y_r^b + y_s)$. where A_r^b is the cross-section area of bottom geosynthetic reinforcement; y_r^b is the locations of bottom geosynthetic layer from the centroid axis; and y_s is the distance between neutral axis and centroid axis of LTP within the sagging bending moment section. The above-mentioned equation is a quadratic equation in terms of h_s, the value of which determines the location of the neutral axis. Similarly, to establish the neutral axis (h_h) in the hogging region, first moment of the compression area in the LTP (A_h) above the neutral axis with respect to neutral axis must be equal that of the tension area in the transformed geosynthetic layer (nA_r^t) below the neutral axis. To acquire the depth of the neutral axis $(h_s$ or $h_h)$, the solutions of the resulting quadratic equations are found as follows:

$$h = \begin{cases} h_s = \sqrt{\left(\frac{S_r^b}{E_g}\right)^2 + \left[\frac{S_r^b}{E_g}\left(2y_r^b + h\right)\right]} - \left(\frac{S_r^b}{E_g}\right), & -r \leq x \leq +r \qquad \text{(1a)} \\ h_h = \sqrt{\left(\frac{S_r^t}{E_g}\right)^2 + \left[\frac{S_r^t}{E_g}\left(2y_r^t + h\right)\right]} - \left(\frac{S_r^t}{E_g}\right), & \pm r \leq x \leq \pm\frac{s}{2} \qquad \text{(1b)} \end{cases}$$

where h is the thickness of LTP before cracking; h_s and h_h are the locations of neutral axis in sagging moment and hogging moment zones, respectively; y_r^t and y_r^b are the locations of top and bottom geosynthetic layer from the centroid axis, respectively; $S_r^t(= A_r^t E_r^t)$ and $S_r^b(= A_r^b E_r^b)$ are the tensile stiffness of top and bottom geosynthetic layers, respectively; E_r^t and E_r^b are the Young's moduli of top and bottom reinforcements, respectively; E_g is the Young's modulus of the granular material; and A_r^t and A_r^b are the cross-sectional area of top and bottom geosynthetic reinforcements, respectively

After locating the neutral axis, the equivalent bending stiffness of the granular layer with geosynthetic reinforcement (D_s and D_h) is calculated as follows.

(2a)

$$D = \begin{cases} D_s = E_g I_s + S_r^b (y_s + y_r^b)^2, & -r \leq x \leq +r \\ D_h = E_g I_h + S_r^t (y_h + y_r^t)^2, & \pm r \leq x \leq \pm \frac{s}{2} \end{cases} \tag{2b}$$

Although in flexure, the existence of granular materials below/above the neutral axis is omitted, but the same granular material between the neutral axis and the cracks is needed for shear transfer between the geosynthetic reinforcement and the compression zone. Hence, the shear stiffness of the granular fill including geosynthetic reinforcement (C) can be calculated as follows.

$$C = k_{sc} \left\{ \frac{E_g h}{2(1+\nu_g)} + \frac{S_r^t}{2(1+\nu_r^t)} + \frac{S_r^b}{2(1+\nu_r^b)} \right\}, \qquad -\frac{s}{2} \leq x \leq +\frac{s}{2} \tag{3}$$

where y_s and y_h are the distances between neutral axis and centroid axis of LTP within the sagging and hogging bending moment sections, respectively; ν_g, ν_r^t, and ν_r^b are the Poisson's ratios of granular material, top and bottom geosynthetic layers, respectively; D_s and D_h are the equivalent bending stiffness of LTP within the sagging and hogging bending moment sections, respectively; C is the shear stiffness of LTP irrespective of the sagging and hogging bending moments; I_s and I_h are the second moment of inertias of the granular materials within the sagging and hogging bending moment sections, respectively ($I_s = {h_s}^3/3$ and $I_h = {h_h}^3/3$); and k_{sc} is the shear factor suggested by Cowper (1966) and Hutchinson (2001) for the rectangular cross section of a beam.

As the LTP settles on the column improved soft soil, shear stresses are generated in the soft soil. Thus, Winkler foundation model to simulate the soft soil under the LTP would not be suitable in this case as the differential settlement occurs underneath the granular layer. Because of the discontinuity amongst the spring elements, Winkler foundation model cannot consider the shear stress transfer in the soil. Hence, for the sake of realistic modelling of the soft soil, the connectivity of the individual Winkler springs must be achieved through a structural element such as a beam, a shear layer, or a plate. However, this structural element cannot be introduced just below the granular layer. Since the differential settlement of soft soil just underneath the granular layer is very high, large shear stresses are generated in this region. However, since soil is a continuum medium, the differential settlement dissipates over the soil depth, resulting in less shear stresses generated in the soft soil. Therefore, structural elements such as a shear layer must be introduced in combination with the Winkler springs at some distance below the granular layer. Hence, the Kerr foundation model which consists of two spring layers interconnected by a shear layer is adopted to simulate the soft soil. The three-parameter Kerr foundation model consists of two linear spring layers with modulus of subgrade reactions k_u and k_l, interconnected by a shear layer with shear modulus G (as shown in Fig. 1a). Plane strain condition allowing the consideration of a LTP strips of finite length "s" and unit width, is considered. To analyse the LTP, the equilibrium equations (i.e. externally applied loads equal to the sum of the internal element forces at all nodes of a structure) and the compatibility equations (i.e. one or more equations which state either that no gaps exist internally or deflections are consistent with the geometry imposed by the supports) which are the most fundamental equations in structural analysis. Therefore, the concept of “Load-Displacement compatibility method” in the present research is adopted from fundamental laws of physics. Similar concept was implemented by Smith (2005) and Filz and Smith (2007) for design of bridging layers in geosynthetics reinforced embankments. Hence, to satisfy the vertical deformation continuity, the following conditions should be satisfied.

$$w_{LTP} = \begin{cases} w_s^{LTP} = w_s^{us} + w_s^{ls}\,, \qquad -r \le x \le +r & \text{(4a)} \\ w_h^{LTP} = w_h^{us} + w_h^{ls}\,, \qquad \pm r \le x \le \pm \frac{s}{2} & \text{(4b)} \end{cases}$$

where w_s^{LTP} and w_h^{LTP} are the deflections of the LTP in the sagging and hogging regions, respectively; w_s^{us} and w_s^{ls} are the contractions or extensions of the upper and lower springs layers in the sagging region, respectively; w_h^{us} and w_h^{ls} are the contraction or extension of the upper and lower spring layers in the hogging region, respectively. The contact pressures (q) under the LTP as shown in Fig. 1b can be expressed as:

$$q = \begin{cases} q_s = k_u w_s^{us}, & -r \leq x \leq +r \quad (5a) \\ q_h = k_u w_h^{us}, & \pm r \leq x \leq \pm\frac{s}{2} \quad (5b) \end{cases}$$

The governing equation for the Pasternak shear layer as displayed in Fig. 1c is given by:

$$q = \begin{cases} q_s = k_l w_s^{ls} - G w_s^{ls''}, & -r \leq x \leq +r \quad (6a) \\ q_h = k_l w_h^{ls} - G w_h^{ls''}, & \pm r \leq x \leq \pm\frac{s}{2} \quad (6b) \end{cases}$$

where k_u and k_l are the spring constants for upper and lower layers, respectively and G is the shear modulus of soft soil. According to Lagrange's notation, a prime mark denotes a derivative (e.g. $w_s^{ls''} = \frac{d^2 w_s^{ls}}{dx^2}$).

Rearranging Eqs. (5a) and (5b), the relationship between the deflection of the upper soil layer and the contact pressure at the interface of LTP and soft soil can be obtained as below:

$$\frac{k_l}{k_u} q_s - \frac{G}{k_u} q_s'' = k_l w_s^{us} - G w_s^{us''}, \quad -r \leq x \leq +r \quad (7a)$$

and

$$\frac{k_l}{k_u} q_h - \frac{G}{k_u} q_h'' = k_l w_h^{us} - G w_h^{us''}, \quad \pm r \leq x \leq \pm\frac{s}{2} \quad (7b)$$

Combining Eqs. (6a) and (7a) and then substituting the resulting equation in Eq. (4a), leads the relationship between the deflection of the LTP and the contact pressure at the interface of LTP and soft soil in sagging region which is stated in Eq. (8a) (similar steps are applied for Eq. (8b)):

$$\left(1+\frac{k_l}{k_u}\right)q_s-\frac{G}{k_u}{q_s}''=k_l w_s^{LTP}-G{w_s^{LTP}}'' , \qquad -r\le x\le +r \tag{8a}$$

and

$$\left(1+\frac{k_l}{k_u}\right)q_h-\frac{G}{k_u}{q_h}''=k_l w_h^{LTP}-G{w_h^{LTP}}'' , \qquad \pm r\le x\le \pm\frac{s}{2} \tag{8b}$$

The differential equations for a LTP in the plane strain condition adopting membrane reinforced Timoshenko (1921) beam can be rewritten as:

$$D_s {w_s^{LTP}}^{iv}-\frac{D_s}{C}{q_s}''+q_s=p-\frac{D_s}{C}p'', \qquad -r\le x\le +r \tag{9a}$$

and

$$D_h {w_h^{LTP}}^{iv}-\frac{D_h}{C}{q_h}''+q_h=p-\frac{D_h}{C}p'', \qquad \pm r\le x\le \pm\frac{s}{2} \tag{9b}$$

Combining Eqs. (8a) and (9a) yields the governing differential equation of the deflection of the LTP for sagging region (i.e. for $-r\le x\le +r$) which is expressed as below.

$$\left(\frac{GD_s}{k_u}\right){w_s^{LTP}}^{vi}-D_s\left(1+\frac{k_l}{k_u}+\frac{G}{C}\right){w_s^{LTP}}^{iv}+\left(\frac{D_s k_l}{C}+G\right){w_s^{LTP}}''-k_l w_s^{LTP}=$$

$$-\left(\frac{GD_s}{Ck_u}\right)p^{iv}+\left(\frac{D_s}{C}+\frac{D_s k_l}{Ck_u}+\frac{G}{k_u}\right)p''-\left(1+\frac{k_l}{k_u}\right)p \tag{10a}$$

where Roman numerals, as in ${w_s^{LTP}}^{vi}$, ${w_s^{LTP}}^{iv}$, and ${w_s^{LTP}}''$ denote sixth, fourth, and second order derivatives with respect to x, respectively.

Similarly, combining Eqs. (8b) and (9b), the response of LTP in the hogging region (i.e. for $\pm r\le x\le \pm s/2$) can be represented as:

$$\left(\frac{GD_h}{k_u}\right){w_h^{LTP}}^{vi}-D_h\left(1+\frac{k_l}{k_u}+\frac{G}{C}\right){w_h^{LTP}}^{iv}+\left(\frac{D_h k_l}{C}+G\right){w_h^{LTP}}''-k_l w_h^{LTP}=$$

$$-\left(\frac{GD_h}{Ck_u}\right)p^{iv}+\left(\frac{D_h}{C}+\frac{D_h k_l}{Ck_u}+\frac{G}{k_u}\right)p''-\left(1+\frac{k_l}{k_u}\right)p \tag{10b}$$

3. The analytical solutions

In the present study, two-dimensional plane strain analysis has been carried out for column-supported structures. Analytical solutions are obtained for calculating the settlement of the load transfer platform at any arbitrary point for the symmetric loading condition. Fourier series is utilised to consider the symmetric distribution of vertical loading (p) on LTP between the two adjacent columns. Hence, p can be described as:

$$p = P_0 + \sum_{n=1}^{n=\infty} P_n \cos\left(\frac{2n\pi x}{s}\right) \tag{11}$$

where

$$P_0 = \frac{1}{s}\int_{-s/2}^{s/2} f(x)\, dx \;\text{ and }\; P_n = \frac{2}{s}\int_{-s/2}^{s/2} f(x) \cos\left(\frac{2n\pi x}{s}\right) \tag{12}$$

Combining Eqs. (10a) and (11), the following differential equation is governed for Region I (i.e. for $-r \leq x \leq +r$).

$$w_s^{LTP^{vi}} + X_s w_s^{LTP^{iv}} + Y_s w_s^{LTP''} + Z_s w_s^{LTP} = -\left(\frac{k_u+k_l}{GD_s}\right) P_0 -$$

$$\sum_{n=1}^{n=\infty}\left[\left(\frac{k_u+k_l}{GD_s}\right) + \left(\frac{k_u}{GC} + \frac{k_l}{GC} + \frac{1}{D_s}\right)\left(\frac{2n\pi}{s}\right)^2 + \frac{1}{C}\left(\frac{2n\pi}{s}\right)^4\right] P_n \cos\left(\frac{2n\pi x}{s}\right) \tag{13a}$$

Similarly, by substituting Eq. (11) into Eq. (10b), the following differential equation for Region II (i.e. for $\pm r \leq x \leq \pm s/2$) can be derived:

$$w_h^{LTP^{vi}} + X_h w_h^{LTP^{iv}} + Y_h\, w_h^{LTP''} + Z_h w_h^{LTP} = -\left(\frac{k_u+k_l}{GD_h}\right) P_0 -$$

$$\sum_{n=1}^{n=\infty}\left[\left(\frac{k_u+k_l}{GD_h}\right) + \left(\frac{k_u}{GC} + \frac{k_l}{GC} + \frac{1}{D_h}\right)\left(\frac{2n\pi}{s}\right)^2 + \frac{1}{C}\left(\frac{2n\pi}{s}\right)^4\right] P_n \cos\left(\frac{2n\pi x}{s}\right) \tag{13b}$$

where

$$\begin{Bmatrix} X_s = -\frac{1}{G}\left(k_u + k_l + \frac{k_u G}{C}\right) \\ X_h = -\frac{1}{G}\left(k_u + k_l + \frac{k_u G}{C}\right) \end{Bmatrix}; \begin{Bmatrix} Y_s = \frac{k_u k_l}{GC} + \frac{k_u}{D_s} \\ Y_h = \frac{k_u k_l}{GC} + \frac{k_u}{D_h} \end{Bmatrix}; \text{ and } \begin{Bmatrix} Z_s = -\frac{k_u k_l}{GD_s} \\ Z_h = -\frac{k_u k_l}{GD_h} \end{Bmatrix} \tag{14}$$

The governing differential equations (i.e. Eqs. (13a) and (13b)) are sixth order, linear, and nonhomogeneous equations with constant coefficients. To obtain general solutions for the governing differential equations, auxiliary or complementary equations corresponding to the homogeneous equations are solved. The auxiliary equations to the homogeneous equations can be expressed in a generalised form as stated in Eqs. (15a) and (15b) sourcing the solution for the original nonhomogeneous equations with roots a_{s1} to a_{s6} and a_{h1} to a_{h6}. The auxiliary equations corresponding to Eqs. (13a) and (13b) are:

$$a_s{}^6 + X_s a_s{}^4 + Y_s a_s{}^2 + Z_s = 0\,, \qquad -r \le x \le +r \tag{15a}$$

and

$$a_h{}^6 + X_h a_h{}^4 + Y_h a_h{}^2 + Z_h = 0\,, \qquad \pm r \le x \le \pm\frac{s}{2} \tag{15b}$$

For the sake of paper length, detailed calculation steps for the sagging section are explained in details and readers can simply use the same method to obtain the solution for the hogging region. Eq. (15a) is a polynomial equation of degree 6. Therefore, Eq. (15a) has 6 real and/or complex roots (not necessarily distinct). Considering $a_s{}^2 = \mu_s$, the following relation is obtained from Eq. (15a):

$$\mu_s{}^3 + X_s \mu_s{}^2 + Y_s \mu_s + Z_s = 0 \tag{16}$$

Considering $\mu_s = b_s - (X_{\,s}/3)$, Eq. (16) can be rewritten as

$$b_s{}^3 + 3\alpha_s b_s + 2\beta_s = 0 \tag{17}$$

where

$$\alpha_s = \frac{1}{3}\left(Y_s - \frac{X_s{}^2}{3}\right) \text{ and } \beta_s = \frac{1}{2}\left(\frac{2X_s{}^3}{27} - \frac{X_s Y_s}{3} + Z_s\right) \tag{18}$$

There are many solution types to Eq. (13a) depending on the auxiliary parameter Δ_s, where:

$$\Delta_s = -108\left(\alpha_s{}^3 + \beta_s{}^2\right) \tag{19}$$

It is well established in the literature (Avramidis and Morfidis, 2006; Morfidis, 2007) that the most common solution case corresponding to the positive sign of the auxiliary parameter Δ_s is when $\Delta_s < 0$. Thus Eq. (19) converts to $\alpha_s{}^3 + \beta_s{}^2 > 0$ with one real and two conjugate complex roots. The real root (μ_{s1}) is as following:

$$\mu_{s1} = -\frac{X_s}{3} + \sqrt[3]{-\beta_s + \sqrt{\Delta_s}} + \sqrt[3]{-\beta_s - \sqrt{\Delta_s}} \tag{20a}$$

and the two complex roots (μ_{s2} and μ_{s3}) are as below:

$$\mu_{s2} = -\frac{X_s}{3} - \frac{1}{2}\left(\sqrt[3]{-\beta_s + \sqrt{\Delta_s}} + \sqrt[3]{-\beta_s - \sqrt{\Delta_s}}\right) + i\frac{\sqrt{3}}{2}\left(\sqrt[3]{-\beta_s + \sqrt{\Delta_s}} - \sqrt[3]{-\beta_s - \sqrt{\Delta_s}}\right) \tag{20b}$$

and

$$\mu_{s3} = -\frac{X_s}{3} - \frac{1}{2}\left(\sqrt[3]{-\beta_s + \sqrt{\Delta_s}} + \sqrt[3]{-\beta_s - \sqrt{\Delta_s}}\right) - i\frac{\sqrt{3}}{2}\left(\sqrt[3]{-\beta_s + \sqrt{\Delta_s}} - \sqrt[3]{-\beta_s - \sqrt{\Delta_s}}\right) \tag{20c}$$

If six roots of Eq. (15a) are known as a_{sj} where $j = 1{-}6$, then the solution of the homogeneous equation (Eq. (15a)) can be tabulated as:

$$a_{sj} = \begin{cases} +\sqrt{\mu_{s1}} = e^{\delta_s x}\ , & \text{Real root} \\ -\sqrt{\mu_{s1}} = e^{-\delta_s x}\ , & \text{Real root} \\ +\sqrt{\mu_{s2}} = e^{-\varepsilon_s x}\cos\sigma_s x\ , & \text{Complex root} \\ +\sqrt{\mu_{s3}} = e^{-\varepsilon_s x}\sin\sigma_s x\ , & \text{Complex root} \\ -\sqrt{\mu_{s2}} = e^{\varepsilon_s x}\cos\sigma_s x\ , & \text{Complex root} \\ -\sqrt{\mu_{s3}} = e^{\varepsilon_s x}\sin\sigma_s x\ , & \text{Complex root} \end{cases} \tag{21}$$

where

$$\begin{cases} \delta_s = \pm\sqrt{-\frac{X_s}{3} + \sqrt[3]{-\beta_s + \sqrt{\Delta_s}} + \sqrt[3]{-\beta_s - \sqrt{\Delta_s}}} \\ \varepsilon_s = \sqrt{\frac{1}{2}\left(\sqrt{{m_s}^2 + {n_s}^2} + m_s\right)} \\ \sigma_s = \sqrt{\frac{1}{2}\left(\sqrt{{m_s}^2 + {n_s}^2} - m_s\right)} \end{cases} \tag{22}$$

Following equations can be used to obtain m_s and n_s required in Eq. (22).

$$m_s = -\frac{1}{2}\left(\frac{2X_s}{3} + \sqrt[3]{-\beta_s + \sqrt{\Delta_s}} + \sqrt[3]{-\beta_s - \sqrt{\Delta_s}}\right) \tag{23a}$$

and

$$n_s = \frac{\sqrt{3}}{2}\left(\sqrt[3]{-\beta_s + \sqrt{\Delta_s}} - \sqrt[3]{-\beta_s - \sqrt{\Delta_s}}\right) \tag{23b}$$

To obtain the general solutions for Eqs. (13a) and (13b), the particular solutions (y_p) must be found. Thus, trial forms for the particular integral are assumed for the two differential equations with different constants which are presented in Eqs.(24a) and (24b).

$$y_p = \begin{cases} y_{ps} = W_s \cos\left(\frac{2n\pi x}{s}\right), & -r \leq x \leq +r \quad (24a) \\ y_{ph} = W_h \cos\left(\frac{2n\pi x}{s}\right), & \pm r \leq x \leq \pm\frac{s}{2} \quad (24b) \end{cases}$$

where W_s and W_h are the arbitrary constants for the sagging and hogging regions, respectively. These trial functions are then substituted into the corresponding differential equations (i.e. Eqs. (13a) and (13b)) and the constants resulting in particular solutions are obtained. Subsequently, the following expressions are obtained for the particular solutions:

$$y_p = \begin{cases} y_{ps} = \left(\frac{k_u+k_l}{k_u k_l}\right) P_0 + \sum_{n=1}^{n=\infty} p_{ns} \cos\left(\frac{2n\pi x}{s}\right), & -r \leq x \leq +r \quad (25a) \\ y_{ph} = \left(\frac{k_u+k_l}{k_u k_l}\right) P_0 + \sum_{n=1}^{n=\infty} p_{nh} \cos\left(\frac{2n\pi x}{s}\right), & \pm r \leq x \leq \pm\frac{s}{2} \quad (25b) \end{cases}$$

where

$$p_{ns} = \frac{P_n\left[\frac{1}{k_u}\left(\frac{2n\pi}{s}\right)^4 + \frac{k_u}{GD_s}\left(\frac{D_s}{C} + \frac{D_s k_l}{k_u C} + \frac{G}{k_u}\right)\left(\frac{2n\pi}{s}\right)^2 + \frac{(k_u+k_l)}{GD_s}\right]}{\left(\frac{2n\pi}{s}\right)^6 + \frac{1}{G}\left(k_u + k_l + \frac{k_u G D_s}{C}\right)\left(\frac{2n\pi}{s}\right)^4 + \frac{k_u}{D_s}\left(1 + \frac{k_l D_s}{GC}\right)\left(\frac{2n\pi}{s}\right)^2 + \frac{k_u k_l}{GD_s}} \quad (26a)$$

and

$$p_{nh} = \frac{P_n\left[\frac{1}{k_u}\left(\frac{2n\pi}{s}\right)^4 + \frac{k_u}{GD_h}\left(\frac{D_h}{C} + \frac{D_h k_u}{k_1 C} + \frac{G}{k_u}\right)\left(\frac{2n\pi}{s}\right)^2 + \frac{(k_u+k_l)}{GD_h}\right]}{\left(\frac{2n\pi}{s}\right)^6 + \frac{1}{G}\left(k_u + k_l + \frac{k_u G D_h}{C}\right)\left(\frac{2n\pi}{s}\right)^4 + \frac{k_u}{D_h}\left(1 + \frac{k_l D_h}{GC}\right)\left(\frac{2n\pi}{s}\right)^2 + \frac{k_u k_l}{GD_h}} \quad (26b)$$

Finally, using the superposition principle, the solution of the governing differential equation (i.e. Eq. (13a)) for the settlement of the LTP with symmetric loading in the sagging region (i.e. for $-r \leq x \leq +r$) can be written as follows:

$$w_s^{LTP} = c_1 e^{-\delta_s x} + c_2 e^{\delta_s x} + e^{-\varepsilon_s x}(c_3 \cos\sigma_s x + c_4 \sin\sigma_s x) +$$

$$e^{\varepsilon_s x}(c_5 \cos\sigma_s x + c_6 \sin\sigma_s x) + \left(\frac{k_u + k_l}{k_u k_l}\right) P_0 + \sum_{n=1}^{n=\infty} p_{ns} \cos\left(\frac{2n\pi x}{s}\right) \qquad (27a)$$

Similarly, the solution of the governing differential equation for the deflection of the LTP with symmetric loading in the hogging region (i.e. for $\pm r \leq x \leq \pm s/2$) is given by:

$$w_h^{LTP} = d_1 e^{-\delta_h x} + d_2 e^{\delta_h x} + e^{-\varepsilon_h x}(d_3 \cos\sigma_h x + d_4 \sin\sigma_h x) +$$

$$e^{\varepsilon_h x}(d_5 \cos\sigma_h x + d_6 \sin\sigma_h x) + \left(\frac{k_u + k_l}{k_u k_l}\right) P_0 + \sum_{n=1}^{n=\infty} p_{nh} \cos\left(\frac{2n\pi x}{s}\right) \qquad (27b)$$

where δ_h, ε_h, and σ_h for the hogging section can be calculated following the similar procedures as described for the sagging region in Eqs. (22) and (23a). Once the deflections of LTP at different locations are obtained using Eqs. (27a) and (27b), the rotational angles of cross sections of LTP, the shear forces generated in LTP, the bending moments developed in LTP, and the tension mobilised in the geosynthetic reinforcement for each section can be obtained as set out in the following sections.

Deflection of the shear layer embedded in the Kerr foundation can be expressed in terms of w_{LTP}. According to Eqs. (4a) and (5a):

$$q_s = k_u(w_s^{LTP} - w_s^{ls}) \ , \qquad -r \leq x \leq +r \qquad (28)$$

Then combination of Eqs. (28) and (9a) yields the following equation.

$$w_s^{ls} = U_1 {w_s^{LTP}}^{iv} - \left(\frac{U_1 k_u}{C}\right) {w_s^{LTP}}'' + \left(\frac{U_1 k_u k_l}{CG} + 1\right) w_s^{LTP} - \left(\frac{U_1}{D_s}\right) p +$$

$$\left(\frac{U_1}{C}\right) p'' , \ -r \leq x \leq +r \qquad (29a)$$

Similarly, for the hogging region, deflection of the shear layer within the Kerr foundation is given by:

$$w_{h^{ls}} = U_2 {w_h^{LTP}}^{iv} - \left(\frac{U_2 k_u}{C}\right) {w_h^{LTP}}'' + \left(\frac{U_2 k_u k_l}{CG} + 1\right) w_h^{LTP} - \left(\frac{U_2}{D_h}\right) p +$$

$$\left(\frac{U_2}{C}\right) p'' , \ \pm r \leq x \leq \pm \frac{s}{2} \qquad (29b)$$

where

$$U_1 = \frac{D_s CG}{k_u[CG - D_s(k_u + k_l)]} \text{ and } U_2 = \frac{D_h CG}{k_u[CG - D_h(k_u + k_l)]} \quad (30)$$

3.1. *Rotation of LTP*

According to the direction of bending moment (i.e. sagging or hogging), the rotation of the cross section of LTP (reinforced Timoshenko beam model) on the Kerr foundation model is given by:

$$\theta_{LTP} = \begin{cases} \theta_s^{LTP} = \frac{D_s}{C} w_s^{LTP'''} + w_s^{LTP'} - \frac{D_s}{C^2} q_s' + \frac{D_s}{C^2} p', \ -r \le x \le +r & (31a) \\ \theta_h^{LTP} = \frac{D_h}{C} w_h^{LTP'''} + w_h^{LTP'} - \frac{D_h}{C^2} q_h' + \frac{D_h}{C^2} p', \ \pm r \le x \le \pm\frac{s}{2} & (31b) \end{cases}$$

Substituting Eqs. (5a) and (11) into Eq. (31a) and then utilising Eq. (27a) lead to the governing equation for rotation of the cross section of LTP in sagging region which is written below.

$$\theta_s^{LTP} = -c_1 A_1 \delta_s e^{-\delta_s x} + c_2 A_1 \delta_s e^{\delta_s x} - c_3 e^{-\varepsilon_s x}(B_1 \sin\sigma_s x - C_1 \cos\sigma_s x) + c_4 e^{-\varepsilon_s x}(C_1 \sin\sigma_s x + B_1 \cos\sigma_s x) - c_5 e^{\varepsilon_s x}(B_1 \sin\sigma_s x + C_1 \cos\sigma_s x) - c_6 e^{\varepsilon_s x}(C_1 \sin\sigma_s x - B_1 \cos\sigma_s x) - \sum_{n=1}^{n=\infty} \left\{ \left[D_1 + E_1 \left(\frac{2n\pi}{s}\right)^4 - F_1 \left(\frac{2n\pi}{s}\right)^2 \right] p_{ns} + \left[\left(\frac{GF_1 {D_s}^2}{C^2}\right)\left(\frac{2n\pi}{s}\right)^2 + \left[\left(\frac{GF_1 D_s}{C}\right) + \frac{D_s}{C^2}\right] \right] P_n \right\} \left(\frac{2n\pi}{s}\right) \sin\left(\frac{2n\pi x}{s}\right) \quad (32a)$$

In the same way, combining Eqs. (5b), (11), (27b), and (31b), the governing equation for rotation of the cross section of LTP in hogging region can be expressed as:

$$\theta_h^{LTP} = -d_1 A_2 \delta_h e^{-\delta_h x} + d_2 A_2 \delta_h e^{\delta_h x} - d_3 e^{-\varepsilon_h x}(B_2 \sin\sigma_h x - C_2 \cos\sigma_h x) + d_4 e^{-\varepsilon_h x}(C_2 \sin\sigma_h x + B_2 \cos\sigma_h x) - d_5 e^{\varepsilon_h x}(B_2 \sin\sigma_h x + C_2 \cos\sigma_h x) - d_6 e^{\varepsilon_h x}(C_2 \sin\sigma_h x - B_2 \cos\sigma_h x) - \sum_{n=1}^{n=\infty} \left\{ \left[D_2 + E_2 \left(\frac{2n\pi}{s}\right)^4 - F_2 \left(\frac{2n\pi}{s}\right)^2 \right] p_{nh} + \left[\left(\frac{GF_2 {D_h}^2}{C^2}\right)\left(\frac{2n\pi}{s}\right)^2 + \left[\left(\frac{GF_2 D_h}{C}\right) + \right.\right.\right. \quad (32b)$$

$$\left.\left.\frac{D_h}{C^2}\right]\right] P_n \Bigg\} \left(\frac{2n\pi}{s}\right) \sin\left(\frac{2n\pi x}{s}\right)$$

where

$$\begin{cases} A_1 = \delta_s\left({\delta_s}^4 E_1 + {\delta_s}^2 F_1 + D_1\right) \\ A_2 = \delta_h\left({\delta_h}^4 E_2 + {\delta_h}^2 F_2 + D_2\right) \end{cases} \tag{33a}$$

$$\begin{cases} B_1 = \sigma_s[E_1({\sigma_s}^4 - 10{\varepsilon_s}^2{\sigma_s}^2 + 5{\varepsilon_s}^4) + F_1(3{\varepsilon_s}^2 - {\sigma_s}^2) + D_1] \\ B_2 = \sigma_h[E_2({\sigma_h}^4 - 10{\varepsilon_h}^2{\sigma_h}^2 + 5{\varepsilon_h}^4) + F_2(3{\varepsilon_h}^2 - {\sigma_h}^2) + D_2] \end{cases} \tag{33b}$$

$$\begin{cases} C_1 = -\varepsilon_s[E_1({\varepsilon_s}^4 - 10{\varepsilon_s}^2{\sigma_s}^2 + 5{\sigma_s}^4) + F_1({\varepsilon_s}^2 - 3{\sigma_s}^2) + D_1] \\ C_2 = -\varepsilon_h[E_2({\varepsilon_h}^4 - 10{\varepsilon_h}^2{\sigma_h}^2 + 5{\sigma_h}^4) + F_2({\varepsilon_h}^2 - 3{\sigma_h}^2) + D_2] \end{cases} \tag{33c}$$

$$\begin{cases} D_1 = 1 - \left(\frac{k_u k_l G_1 {D_s}^2}{C^2}\right) \\ D_2 = 1 - \left(\frac{k_u k_l G_2 {D_h}^2}{C^2}\right) \end{cases} \tag{33d}$$

$$\begin{cases} E_1 = -\frac{G G_1 {D_s}^2}{C} \\ E_2 = -\frac{G G_2 {D_h}^2}{C} \end{cases} \tag{33e}$$

$$\begin{cases} F_1 = \frac{D_s}{C}\left(1 + \frac{G k_u G_1 D_s}{C}\right) \\ F_2 = \frac{D_h}{C}\left(1 + \frac{G k_u G_2 D_h}{C}\right) \end{cases} \tag{33f}$$

and

$$\begin{cases} G_1 = \frac{D_s}{C} - \frac{D_s}{C^2}\frac{G k_u}{k_u + k_l} \\ G_2 = \frac{D_h}{C} - \frac{D_h}{C^2}\frac{G k_u}{k_u + k_l} \end{cases} \tag{33g}$$

3.2. Bending moment and shear force in LTP

According to the theory of Timoshenko beam (1921), the relationship between moment and the rate of rotation angle change can be written as:

$$M_{LTP} = \begin{cases} M_s^{LTP} = -D_s \theta_s^{LTP'}, \ -r \le x \le +r & \text{(34a)} \\ M_h^{LTP} = -D_h \theta_h^{LTP'}, \ \pm r \le x \le \pm\frac{s}{2} & \text{(34b)} \end{cases}$$

By substituting Eq. (32a) into Eq.(34a), the governing equations for the bending moments in the LTP can be obtained as:

$$M_s^{LTP} = -D_s\Big\{c_1A_1{\delta_s}^2e^{-\delta_s x} + c_2A_1{\delta_s}^2e^{\delta_s x} + c_3e^{-\varepsilon_s x}(J_1\sin\sigma_s x - I_1\cos\sigma_s x) - c_4e^{-\varepsilon_s x}(I_1\sin\sigma_s x + J_1\cos\sigma_s x) - c_5e^{\varepsilon_s x}(J_1\sin\sigma_s x + I_1\cos\sigma_s x) - c_6e^{\varepsilon_s x}(I_1\sin\sigma_s x - J_1\cos\sigma_s x) - \sum_{n=1}^{n=\infty}\Big\{\Big[D_1 + E_1\left(\frac{2n\pi}{s}\right)^4 - F_1\left(\frac{2n\pi}{s}\right)^2\Big]p_{ns} + \Big[\left(\frac{GF_1{D_s}^2}{C^2}\right)\left(\frac{2n\pi}{s}\right)^2 + \Big[\left(\frac{GF_1D_s}{C}\right) + \frac{D_s}{C^2}\Big]\Big]P_n\Big\}\left(\frac{2n\pi}{s}\right)^2\cos\left(\frac{2n\pi x}{s}\right)\Big\} \quad (35a)$$

The following can be derived from Eqs. (32b) and (34b):

$$M_h^{LTP} = -D_h\Big\{d_1A_2{\delta_h}^2e^{-\delta_2 x} + d_2A_2{\delta_h}^2e^{\delta_h x} + d_3e^{-\varepsilon_h x}(J_2\sin\sigma_h x - I_2\cos\sigma_h x) - d_4e^{-\varepsilon_h x}(I_2\sin\sigma_h x + J_2\cos\sigma_h x) - d_5e^{\varepsilon_h x}(J_2\sin\sigma_h x + I_2\cos\sigma_h x) - d_6e^{\varepsilon_h x}(I_2\sin\sigma_h x - J_2\cos\sigma_h x) - \sum_{n=1}^{n=\infty}\Big\{\Big[D_2 + E_2\left(\frac{2n\pi}{s}\right)^4 - F_2\left(\frac{2n\pi}{s}\right)^2\Big]p_{nh} + \Big[\left(\frac{GF_2{D_h}^2}{C^2}\right)\left(\frac{2n\pi}{s}\right)^2 + \Big[\left(\frac{GF_2D_h}{C}\right) + \frac{D_h}{C^2}\Big]\Big]P_n\Big\}\left(\frac{2n\pi}{s}\right)^2\cos\left(\frac{2n\pi x}{s}\right)\Big\} \quad (35b)$$

According to the direction of bending moment (i.e. sagging or hogging) the shear force in LTP can be expressed as:

$$V_{LTP} = \begin{cases} V_s^{LTP} = C\left({w_s^{LTP}}' - \theta_s^{LTP}\right), & -r \le x \le +r \quad (36a) \\ V_h^{LTP} = C\left({w_h^{LTP}}' - \theta_h^{LTP}\right), & \pm r \le x \le \pm\frac{s}{2} \quad (36b) \end{cases}$$

By substituting Eqs. (27a) and (32a) into Eq.(36a), the shear forces developed in the LTP can be obtained as:

$$V_s^{LTP} = C\Big\{c_1K_1\delta_s e^{-\delta_s x} - c_2K_1\delta_s e^{\delta_s x} - c_3e^{-\varepsilon_s x}(M_1\sin\sigma_s x + L_1\cos\sigma_s x) - c_4e^{-\varepsilon_s x}(L_1\sin\sigma_s x - M_1\cos\sigma_s x) - c_5e^{\varepsilon_s x}(M_1\sin\sigma_s x - L_1\cos\sigma_s x) + \quad (37a)$$

$$c_6 e^{\varepsilon_s x}(L_1 \sin \sigma_s x + M_1 \cos \sigma_s x) + \sum_{n=1}^{n=\infty} \left[D_1 + E_1 \left(\frac{2n\pi}{s}\right)^4 - F_1 \left(\frac{2n\pi}{s}\right)^2 - 1 \right] p_{ns} + \left[\left(\frac{GF_1 {D_s}^2}{C^2}\right) \left(\frac{2n\pi}{s}\right)^2 + \left[\left(\frac{GF_1 D_s}{C}\right) + \frac{D_s}{C^2} \right] \right] P_n \left(\frac{2n\pi}{s}\right) \sin \left(\frac{2n\pi x}{s}\right) \Bigg\}$$

Correspondingly, substituting Eqs. (27b) and (32b) into Eq.(36b), the shear forces developed in the LTP in hogging region can be obtained as:

$$V_h^{LTP} = C \Bigg\{ d_1 K_2 \delta_h e^{-\delta_h x} - d_2 K_2 \delta_h e^{\delta_h x} - d_3 e^{-\varepsilon_h x}(M_2 \sin \sigma_h x + L_2 \cos \sigma_h x) - d_4 e^{-\varepsilon_h x}(L_2 \sin \sigma_h x - M_2 \cos \sigma_h x) - d_5 e^{\varepsilon_h x}(M_2 \sin \sigma_h x - L_2 \cos \sigma_h x) + d_6 e^{\varepsilon_h x}(L_2 \sin \sigma_h x + M_2 \cos \sigma_h x) + \sum_{n=1}^{n=\infty} \left[D_2 + E_2 \left(\frac{2n\pi}{s}\right)^4 - F_2 \left(\frac{2n\pi}{s}\right)^2 - 1 \right] p_{nh} + \left[\left(\frac{GF_2 {D_h}^2}{C^2}\right) \left(\frac{2n\pi}{s}\right)^2 + \left[\left(\frac{GF_2 D_h}{C}\right) + \frac{D_h}{C^2} \right] \right] P_n \left(\frac{2n\pi}{s}\right) \sin \left(\frac{2n\pi x}{s}\right) \Bigg\} \quad (37b)$$

where

$$\begin{Bmatrix} I_1 = \varepsilon_s C_1 + \sigma_s B_1 \\ I_2 = \varepsilon_h C_2 + \sigma_h B_2 \end{Bmatrix} \quad (38a)$$

$$\begin{Bmatrix} J_1 = \varepsilon_s B_1 - \sigma_s C_1 \\ J_2 = \varepsilon_h B_2 - \sigma_h C_2 \end{Bmatrix} \quad (38b)$$

$$\begin{Bmatrix} K_1 = \delta_s - A_1 \\ K_2 = \delta_s - A_2 \end{Bmatrix} \quad (38c)$$

$$\begin{Bmatrix} L_1 = \varepsilon_s + C_1 \\ L_2 = \varepsilon_h + C_2 \end{Bmatrix} \quad (38d)$$

and

$$\begin{Bmatrix} M_1 = \sigma_s - B_1 \\ M_2 = \sigma_h - B_2 \end{Bmatrix} \quad (38e)$$

3.3. Tension in geosynthetic reinforcement

Tension mobilised in the geosynthetic reinforcement is the product of axial strain in the geosynthetic reinforcement (which is assumed to be equal to the strain developed in the LTP at the location of geosynthetic reinforcement) and the tensile stiffness of the geosynthetic reinforcement. Following the Timoshenko beam theory and depending on the bending moment directions, the tension mobilised in the geosynthetic reinforcement can be expressed as follows:

$$T = \begin{cases} -S_r^b(y_r^b + y_s)\theta_s^{LTP'}, & -r \le x \le +r \qquad (39a) \\ -S_r^t(y_r^t + y_h)\theta_h^{LTP'}, & \pm r \le x \le \pm\frac{s}{2} \qquad (39b) \end{cases}$$

where y_r^t and y_r^b are the distances from the top and bottom geosynthetic layer to the centroid axis, respectively as shown in Fig. 2b; y_s and y_h are the distances between neutral axis and centroid axis of LTP within the sagging and hogging moment sections, respectively as shown in Figs. 2b−c; and S_r^t and S_r^b are the tensile stiffnesses of top and bottom geosynthetic reinforcements, respectively.

3.4. Pressure distribution under LTP

Combining Eqs. (4a), (7a), and (9a), the pressure distribution under the LTP for $-r \le x \le +r$ can be obtained as below:

$$q_s = \frac{GCD_s}{[D_s(k_u+k_l)-GC]} w_s^{LTP^{iv}} - \frac{k_u D_s G}{[D_s(k_u+k_l)-GC]} w_s^{LTP''} + \frac{k_u k_l D_s}{[D_s(k_u+k_l)-GC]} w_s^{LTP} - \frac{GC}{[D_s(k_u+k_l)-GC]} p + \frac{D_s GC}{[D_s(k_u+k_l)-GC]} p'' \qquad (40a)$$

Similarly, from Eqs. (4b), (7b), and (9b), the pressure distribution under the LTP for $\pm r \le x \le \pm s/2$ can be expressed as:

$$q_h = \frac{GCD_h}{[D_h(k_u+k_l)-GC]} w_h^{LTP^{iv}} - \frac{k_u D_h G}{[D_h(k_u+k_l)-GC]} w_h^{LTP''} + \frac{k_u k_l D_h}{[D_h(k_u+k_l)-GC]} w_h^{LTP} - \frac{GC}{[D_h(k_u+k_l)-GC]} p + \frac{D_h GC}{[D_h(k_u+k_l)-GC]} p'' \qquad (40b)$$

3.5. Boundary and continuity conditions

Referring to Eqs. (27a) and (27b), there are twelve constants of integration (c_1 to c_6 and d_1 to d_6) and one unknown length (r) that can be estimated using the boundary and continuity conditions. Due to symmetric loading, at the middle of loaded region, the shear force and the slope of the deflected LTP are zero. Additionally, it is presumed that at the column location, the shear force produced in LTP is equivalent to the reaction force from the column. It is also assumed here that due to inclusion of the geosynthetic reinforcement in LTP and continuity of LTP above the column, LTP will not be rotating at the column support. Summary of the above-mentioned boundary conditions are expressed in Eq. (41).

$$\text{at } x = 0, \begin{cases} V_s^{LTP} = 0 \\ w_s^{LTP'} = 0 \end{cases} \quad \text{and} \quad \text{at } x = \frac{s}{2}, \begin{cases} V_h^{LTP} = -(K_c)_{eq} w_h^{LTP} \\ \theta_h^{LTP} = 0 \end{cases} \tag{41}$$

where $(K_c)_{eq}$ is the equivalent modulus of subgrade reaction for a column in a plane strain condition (kN/m) which can be calculated as Eq. (42).

$$(K_c)_{eq} = \frac{(E_c)_{eq}}{H_c} \times \frac{A_c}{s} \tag{42}$$

where A_c is the area of the column in plane strain condition (i.e. $A_c = s \times d$); s and d are the clear spacing and the diameter of the column, respectively as shown in Fig. 3a; H_c is the length of column; and $(E_c)_{eq}$ is the equivalent elastic modulus of the column wall in plane strain condition. Since in the field, discrete columns are placed in a square or triangular pattern, the equivalent plane strain material stiffness must be determined for the two-dimensional plane strain modeling. In the literature, there are two approaches for plane strain equivalent conversion (Tan et al., 2008). In the first approach, the width of the column (in plane-strain condition) can be taken equal to the diameter of the column (in axisymmetric condition). However, the material stiffness in axisymmetric model should be converted to equivalent plane-strain material stiffness by the suggested relationship based on the matching of the column–soil composite stiffness. This approach was adopted by Huang et al., (2009) where the equivalent elastic modulus and cohesion of the deep mixing walls were calculated during the investigation of coupled mechanical and hydraulic modelling of geosynthetic-reinforced column-supported embankments. In the second approach, geometrical conversion can be done to obtain similar response in both axisymmetric and plane-strain conditions as adopted by Tan et al. (2008). In this study, first approach to convert a 3D or axisymmetric model into an equivalent plane-strain model is adopted. The equivalent modulus is calculated using the area replacement ratio as stated by Huang et al. (2009) as follows:

$$(E_c)_{eq} = E_c a_r + E_s(1 - a_r) \tag{43}$$

where E_c and E_s denote the elastic moduli of the column and soft soil, respectively; while a_r is the area replacement ratio. Similar approach (i.e. first approach) was adopted by Huang et al. (2009) and Deb and Mohapatra (2013) where deep mixing columns and stone columns supported embankments were analysed in plane-strain condition in which the equivalent plane-strain material stiffness of column was determined using the suggested relationship based on the matching of the column–soil composite stiffness.

On the other hand, the effective cross section of the LTP in the sagging region (the left side of point "A" as shown in Fig. 2a) is not the same as the hogging region (right side of point "A"). Hence, the deflections and internal forces in the LTP beam should be represented by two separate functions. However, the deflection curve and internal forces of LTP are physically continuous at point "A" and therefore the continuity conditions for the deflections and moments must be satisfied at point "A". Each of these continuity conditions yields to an equation for evaluating the unknowns. The continuity conditions can be summarised as below:

$$\text{at } x = r \text{ (Point "A")}, \quad \begin{cases} w_s^{LTP} = w_h^{LTP} \\ \theta_s^{LTP} = \theta_h^{LTP} \\ M_s^{LTP} = 0 \\ M_h^{LTP} = 0 \\ V_s^{LTP} = V_h^{LTP} \end{cases} \tag{44}$$

To obtain the continuity conditions for the shear layer in Kerr model, similar continuity conditions can be applied at a distance “r” (i.e. at point “A”) from the symmetry line since in this study 1-D settlement of soft soil has been considered.

$$\text{at } x = r, \quad \begin{cases} w_s^{ls} = w_h^{ls} \\ w_s^{ls'} = w_h^{ls'} \end{cases} \tag{45}$$

Similar to LTP, at the column location, it is assumed that the shear force developed in shear layer is equal to the reaction force from the column. Hence, the varied shear strain along the column length is considered in this study. In addition, as a result of symmetricity, at the mid span shear force in the shear layer should be zero. Thus, the boundary conditions of the shear layer can be summarised as below.

$$\text{at } x = \frac{s}{2} (\text{i. e. at column location}), \; V_h^{ls} = (K_c)_{eq} \left(\frac{G}{C}\right) w_h^{ls} \quad \text{and}$$

$$\text{at } x = 0 (\text{i. e. at mid} - \text{span}), \quad w_s^{ls'} = 0 \tag{46}$$

Replacing the expressions for deflection, rotation of the cross section, moment, and shear force of LTP and the shear layer from Eqs. (27), (32), (35), (37), and (29) respectively into the boundary and the continuity conditions (Eqs. (41) and (44)−(46)) yields thirteen algebraic equations which are summarised in Appendix. Once all the constants of integration and unknown lengths are determined by solving the simultaneous equations, then the deflections, bending moments, shear forces, rotations of the LTP, and mobilised tension in the geosynthetic reinforcement at any point in the LTP can be determined.

Although the overall behaviour of LTP due to bending and shear actions on a soft soil foundation can be predicted using the proposed mechanical model, it should be noted that possible pull-out resistance force of geosynthetic reinforcement, permeability of soft soil, and cyclic loading can significantly affect the performance of soft soil (Indraratna et al., 2005, Suksiripattanapong et al., 2012, Indraratna et al., 2013b).

4. Results and discussions

Due to symmetry, only half of the problem is considered for the parametric study. Based on the formulations and for the sake of convenience and practical use, all the algebraic equations have been programmed in MATLAB R2016b (MathWorks) and the results are presented graphically. Similar to Maheshwari and Viladkar (2009), Zhang et al. (2012b), and Lei et al. (2016), to evaluate the accuracy of implementation of the Kerr foundation model as the soft soil model, the response of double layer geosynthetic reinforced LTP, the tension mobilised in the geosynthetic reinforcement, and stress concentration ratio are compared with the results gained from the Pasternak and the Winkler foundation models. Maheshwari and Viladkar (2009) developed a mechanical model for geosynthetic reinforced soil–foundation system subjected to strip loading and carried out a parametric study to understand the effect of various parameters influencing the response of such a system without validating the proposed model with field or experimental results. Zhang et al. (2012b) proposed a mechanical model of geocell mattress subjected to symmetric loads and the presented solution was verified through comparison with the other existing published solutions namely Zhang et al. (2010) and Qu (2009). Lei et al. (2016) derived an analytical solution to predict consolidation with vertical drains under impeded drainage boundary conditions and multi-ramp surcharge loading. To verify the validity and accuracy of the proposed analytical solution, the results calculated from the proposed solution were compared to those given by the analytical solution of Gray (1944). As far as the maximum settlement of LTP and tension mobilised in the geosynthetic reinforcement (GR) are concerned, the parametric studies have been carried out to show the effects of various parameters on the maximum settlement of LTP and tension mobilised in the geosynthetic reinforcement when the soft soil is idealised by the Kerr foundation model. In this study, mobilised tension in the reinforcement is expressed as a normalised form (T/T_y) assuming ultimate or yield strength of geosynthetic reinforcement is 10% of tensile stiffness of geosynthetic (i.e. T_y = 10%×S_r). Additionally, the results of a double layer geosynthetic reinforced granular fill are compared with a single layer geosynthetic reinforced granular fill. Most of the guidelines adopt single layer of geosynthetics, whereas in practice, it is often common to use two or three layers of geosynthetics. However, to reduce the thickness of LTP, use of single layer but stronger geosynthetic reinforcement may be a good option. Thus, the intention of this parametric study is to investigate whether the use of one stronger geosynthetic layer (e.g. 1×2000 kN/m) with the equivalent stiffness of two weaker geosynthetic layers (e.g. 2×1000 kN/m), results in the same settlement of LTP and the tension of the geosynthetic reinforcement when compared to two weaker geosynthetic layers or not. For the sake of reasonable comparison, similar overall tensile stiffness due to the geosynthetic layers is adopted. For example, 2×1000 kN/m tensile stiffness of geosynthetics for the double layer is compared with 1×2000 kN/m tensile stiffness of a single layer geosynthetics. For two layers' case, geosynthetic reinforcement is placed such that the reinforcement layers equally divide the granular fill layer while the one layer of geosynthetic layer is simply placed at the centre of granular layer for the single layer case. It has been noticed in the literature that many researchers placed the single layer of geosynthetic reinforcement at the mid-level of LTP in their studies (Liu et al., 2007; Nunez et al., 2013). However, it should be noted that geosynthetics can be placed at any level of LTP in case of single layer analysis in the proposed mechanical model. For practical application purposes, the spring constants and the shear modulus of soft soil can be estimated following the procedures proposed by Jones and Xenophontos (1976) for the Kerr foundation model which are summarised as below:

$$k_u = \frac{E_1(1-\nu_1)}{h_1(1-\nu_1-2\nu_1{}^2)}\ ;\ k_l = \frac{E_2\gamma(1-\nu_2)(\sinh\gamma h_2 \cosh\gamma h_2+\gamma h_2)}{2(1-\nu_2-2\nu_2{}^2)\sinh^2\gamma h_2};\ \text{and}$$

$$G = \frac{E_2(\sinh\gamma h_2 \cosh\gamma h_2-\gamma h_2)}{4\gamma(1+\nu_2)\sinh^2\gamma h_2} \qquad (47)$$

where Jones and Xenophontos (1976) assumed a foundation consisting of two layers with elastic coefficients (E_1, ν_1) and (E_2, ν_2) and thicknesses h_1 and h_2 as illustrated in Fig. 1a, respectively. The term γ is a constant, governing the vertical deformation profile. In this study, it is assumed that $\gamma = 0.46$ at the mid-depth of the second layer with thickness h_2 as Kneifati (1985) assumed in his study. Since the analytical solution for homogeneous soil deposit is obtained for one layer only (i.e. $H = 10$ m), and in order to determine the corresponding parameters for the Kerr foundation, (see Eq. (47)), it is assumed that $h_1 = 1$ m; $h_2 = 9$ m; $E_1 = E_2 = E_s = 1000$ kPa; $\nu_1 = \nu_2 = \nu_s = 0.3$. Following the Kerr foundation model, it is presumed that the upper layer of soft soil experiences significant shear deformations (exceeding the shear strength of the soft soil) as commonly modelled by the Winkler foundation. While the lower layer in Kerr foundation model is subjected to both compressive and shear stresses without exceeding the shear strength. Therefore, h_1 and h_2 have been selected in such a way that the maximum shear stress generated in the top section of the soft soil (h_1) reaches the shear strength of the soil, while the shear strength of the soft soil is not exceeded in the bottom part (h_2). It has been noticed that decreasing the depth of upper layer results in larger shear stresses generated in the bottom part of the soft soil (h_2) which exceeds the shear strength of the soft soil. The foregoing solution is evaluated for a uniform load of 200 kPa which includes the self-weight of LTP. The proposed analytical model is a generalised model to analyse the ground stabilised using columns (such as controlled modulus columns, piles, deep soil mixing columns) where load transfer platform is used to enhance the distribution of the load from the super-structures (such as silos, and fuel tanks) to the columns. However, typical properties of controlled modulus columns (CMCs) from a real project in Australia (Highway upgrade, approximately 100 km south of Sydney), is adopted in this study. The material properties used in this study for the baseline case are summarised in Table 1. For the parametric study, one parameter is changed at one time to investigate the influence of that particular parameter. The adopted range of the parameters for the parametric study summarised in Table 2 is considered to cover the typical ranges observed in real projects for the column improved soft soil. In addition, the calculated LTP parameters for double and single layer cases for the baseline case are summarised in Table 3.

4.1. Predictions of Kerr foundation versus other foundation models

In order to verify the validity and accuracy of the proposed analytical solution, the results calculated from the proposed solution for load transfer platform are compared with those given by the analytical solution of the same LTP resting on the Winkler (1867) and the Pasternak (1954) foundations. It is noted that when the shear modulus is equal to zero (i.e. $G = 0$), Eqs. (10a) and (10b) reduce to fourth-order governing differential equations which simulates the response of LTP on Winkler foundation model. Additionally, when the upper spring modulus approaches infinite (i.e. $k_u \to \infty$), Eqs. (10a) and (10b) are reduced to a fourth-order governing differential equations of the LTP on Pasternak foundation model. For the Winkler model, according to Horvath (1983)

$$k_w = \frac{E_s}{H} \tag{48}$$

For the Pasternak model, according to Kerr (1964)

$$k_p = \frac{E_s}{H} \text{ and } G_p = \frac{E_s H}{6(1+\nu_s)} \tag{49}$$

Fig. 3a shows a comparison of the deflection of the LTP adopting the Kerr foundation model to simulate the soft soil against the Winkler and the Pasternak models. There are notable variations in the predictions considering different foundation models. As evident, adopting the Winkler foundation model results in larger deflection of LTP compared to the Kerr foundation model. In contrast, Pasternak model results in less deflection of LTP than the Kerr foundation model. For example, the maximum deflection of LTP adopting the soft soil as Winkler foundation model is about 29 mm, while in Kerr foundation model case the value drops to 25 mm, shown in Fig. 3a. Winkler model only considers the compressibility of the soft soil without any shear resistance. Therefore, the soft soil which is idealised by the Winkler foundation model is prone to an excessive settlement resulting in the largest deformation of the LTP. In contrast, Pasternak foundation model predicts the maximum deflection of LTP of 18 mm, which is 28% less than the corresponding value from the Kerr foundation model as given in Fig. 3a. Since the Pasternak shear layer beneath the LTP is a continuous layer deforming based on elastic shear only, minimum settlement of soil and consequently LTP is occurred. In case of the soft soil idealised by the Kerr foundation, the soil just below the LTP (from the ground surface up to h_1) deforms due to the compressibility of the soft soil only, while in deeper areas both shear resistance and compressibility of the soft soil are contributing to the deformation. Therefore, soft soil simulated with the Kerr foundation behaves stiffer than the Winkler foundation while being softer than the Pasternak foundation. Hence, the Kerr foundation model predicts the deformations more realistically between two upper and lower bounds which are the Winkler and the Pasternak foundation models, respectively.

Fig. 3b shows the predictions of the variation of the rotations of the LTP adopting the soft soil as Kerr, Winkler, and Pasternak foundation models. It is noticed that the Winkler foundation predicts larger LTP rotation compared to the Kerr foundation model. In contrast, the Pasternak model calculates less rotation of LTP compared to the Kerr model. For example, the maximum rotation of LTP when the Kerr foundation model is adopted for the soft soil is -0.03 radians, which increases to -0.04 radians for the Winkler foundation model (i.e. 33% increase) and decreases to -0.019 radians for the Pasternak foundation model (i.e. 37% decrease) as displayed in Fig. 3b. This is since implementing the Winkler model predicts the largest deformation of the LTP (see Fig. 3a); hence the largest rotation of LTP is achieved in the Winkler model. In contrast, adopting the Pasternak model predicts the smallest deformation of LTP (see Fig. 3a), it results in the least rotation of LTP. Accordingly, the Kerr foundation model predicts the rotations more precisely which is between two upper and lower bounds corresponding to the Winkler and the Pasternak foundation models, respectively.

In Fig. 4a, the distribution of the bending moment along the length of the LTP is presented. It is observed that the maximum positive and negative moments in the LTP adopting the Winkler foundation model are approximately 6% and 12% more, respectively, than the corresponding values when the Kerr foundation model is used to simulate the soft soil. In contrast, Pasternak model predicts smaller positive (sagging) and negative (hogging) bending moments in the LTP compared to the Kerr foundation model. As an illustration, the Pasternak foundation model estimates the maximum positive and negative moments in the LTP approximately 35% and 21% less than the corresponding values when the Kerr foundation model is used to simulate the soft soil, respectively, as illustrated in Fig. 4a. Referring to Fig. 3a, since implementing the Winkler model results in the largest deformation of the LTP, the largest moments in the LTP are developed correspondingly. In contrast, the Pasternak model predicts the smallest deformation of LTP (see Fig. 3a), hence it predicts the least moments in the LTP. Accordingly, similar to the deformations reported, the Kerr foundation model calculates the moments more accurately, which are between the upper (i.e. Winkler foundation) and lower bounds(i.e. Pasternak foundation) .

Fig. 4b shows a comparison of the shear forces developed in the LTP using the Kerr foundation model to pretend the soft soil against the Winkler and the Pasternak foundation models. From Fig. 4b it is depicted that the Winkler model estimates larger shear force in LTP as compared to the Kerr model. Whereas, the Pasternak model predicts less shear force in the LTP incomparision to the Kerr model. For example, the maximum shear force in LTP adopting the Kerr foundation model is 131 kN/m, which increases to 140 kN/m and reduces to 128 kN/m in the Winkler and the Pasternak foundation models, respectively. Since adopting the Winkler model predicts larger deflection of LTP compared to the Kerr model (refer to Fig. 3a), shear force induced in the LTP is also greater. On the other hand, adopting the Pasternak model predicts less deflection of LTP incomparision to the Kerr model (see Fig. 3a); hence predicted shear force induced in LTP is also smaller.

Fig. 4c represents the variation of shear forces developed in the soft soil between two columns. As expected, at the mid span, the shear force in the soil is zero due to the symmetric condition while the Kerr and the Pasternak foundation models are used to idealise the soft soil. As evident in Fig. 4c, the shear forces generated in the soft soil for the Pasternak model are greater than those of the Kerr model. Simulating the soft soil as Winkler foundation model, the shear modulus of soft soil is assumed to be zero; therefore, no shear stresses can be predicted in the soft soil as shown in Fig. 4c. When the soft soil is idealised by the Pasternak shear layer, a shear layer is attached to the bottom of the load transfer platform at the ground surface. Hence the soft soil layer underneath the LTP is exposed to shear stresses which may unrealistically exceed the shear strength of the soft soil (violating the elastic assumption used in Pasternak shear layer theory) as shown in Fig. 4c.

Fig. 5a shows the mobilised tension in the top geosynthetic layer adopting the Kerr, Winkler, and Pasternak foundation models to simulate the soft soil. The predicted maximum normalised tensions mobilised in the top geosynthetic layer simulating the soft soil adopting the Kerr and the Winkler foundation models are found to be 0.53 and 0.47 kN/m (i.e. 13% larger than corresponding value when the Kerr model is used); while in the Pasternak foundation case that value is 0.38 (i.e. 20% less than corresponding value while the Kerr model is adopted). Referring to Fig. 3a, as the LTP resting on Winkler foundation deflects greater than the Kerr foundation model, more axial strains and tensions are mobilised in the geosynthetic reinforcement than the Kerr foundation model. In contrast, the Pasternak model results in the smaller deformation of LTP when compare to the Kerr model (see Fig. 3a), hence less axial strains and tensions are mobilised in the geosynthetic reinforcement than the Kerr foundation model. Similarly, the maximum tension in the bottom geosynthetic reinforcement at the mid-span is achieved when the Winkler foundation is adopted while the minimum tension in the bottom geosynthetic reinforcement corresponding to the Pasternak foundation case, which is demonstrated in Fig. 5b. The predicted maximum normalised tension generated in the bottom geosynthetic layer, simulating the soft soil adopting the

Kerr, is 0.23, which rises to 0.27 (i.e. 15% increase) and drops to 0.15 (i.e. 44% decrease) while the Winkler and the Pasternak foundation models are adopted to idealise the soft soil, respectively. Figs. 5a–b also display that larger tensions hence larger strains are generated at the column edge than in the mid-span. Van Eekelen et al. (2015) reported that strains are larger at the edges of the pile caps than in the centre of the GR strips while validating the limit equilibrium models for the arching of basal reinforced piled embankments. However, like a continuous reinforced beam, bottom layer would be under compression at the column location (due to the assumption of small cracks propagation), and since, the geosynthetics only carries tension, there would be no forces mobilised in the geosynthetics. However, when geosynthetics is not stiff enough and granular material is very stiff, then the tension cracks can open and go through low layers of geosynthetics. In that case, the bottom geosynthetic may also attract tension. To consider cracks propagating deep inside the LTP, putting both geosynthetic layers under tension, Eqs. (1a) and (1b) can be used. However, for the selected case study and parametric study, cracks only cross one layer of geosynthetics due to the geometry and material properties used. Hence, bottom geosynthetic was not subjected to tension.

The stress concentration ratios (SCR) when the soft soil is simulated with the Kerr, the Pasternak, and the Winkler foundation models have also been examined in this study. The stress concentration ratio is usually used to analyse the load distribution between the columns and the soil. The higher the stress concentration ratio, the more stress is transferred onto the columns. Since the stress distribution at the interface of LTP and soft soil is not uniform, average stress transferred to the soil is used to determine the stress concentration ratio. The stress concentration ratio can be stated as (Han and Gabr, 2002; Indraratna et al., 2013a):

$$(SCR)_{avg} = \frac{\sigma_c}{\overline{\sigma}_s} \quad (50)$$

where σ_c is the stress transferred to the columns and $\overline{\sigma}_s$ is the average stress transferred to the soil on the surface. The stress concentration ratio for the soft soil idealised as the Winkler foundation is larger than that of the Kerr foundation. Since the behaviour of soft soil under applied load simulated with the Winkler foundation is softer than that of the Kerr foundation model, almost entire applied loads transferred to the column. Very less stresses transferred to the soft soil. Hence very large SCR (SCR = 90) is observed for the Winkler foundation model case. In contrast, the stress concentration ratio for the soft soil idealised as the Pasternak foundation (SCR = 6) is less than that of the Kerr foundation (SCR = 15). Inclusion of the shear layer just beneath the LTP reduces the load transfer to the columns. In other words, soft soil simulated with the Pasternak foundation model behaves stiffer than that of the Kerr foundation model and results in the reduction of the stresses transferred to the column; hence least stress concentration ratio is observed. Similar ranges of stress concentration ratios (as Kerr and Pasternak foundation models) were reported by Han (2001) while stone column reinforced soft soil was analysed.

By comparing the Kerr model to the Winkler and the Pasternak models, it is evident that the combined effect of shear and compression of soft soil results in the most accurate prediction of the response of LTP on soft soil. Since significant differential settlement is expected near the ground surface (i.e. zone h_1 in Fig. 1a), Winkler springs would be more appropriate for simulating the soil near the ground surface. However, in deeper soil layers, experiencing the stress distribution and reduction in the differential settlements, Pasternak shear layer attached to the springs considering both shear and compressive deformations would be more appropriate. Therefore, among these, Kerr foundation model is the most suitable soil foundation model to idealise the mechanistic behaviour of the soft soil beneath LTP. The simplified Winkler model always overpredicts the response of LTP due to the assumption of no shear resistance of soft soil. Whereas, the Pasternak model always underpredicts the deflection of LTP due to large shear resistance near the ground surface.

4.2. *Effects of column spacing*

Fig. 6a represents the effect of column spacing on the maximum settlement of LTP with one layer (1×1000 kN/m) and two layers (2×1000 kN/m) of geosynthetic reinforcement. It is evident from Fig. 6a that as the column spacing increases the maximum settlement of LTP which occurs at the middle of two adjacent columns also increases (as shown in Fig. 3a and as reported by Liu et al., 2015). For example, as the non-dimensional column spacing (s/d) increases from 3 to 3.5 the maximum settlement is increased from 25 mm to 37 mm (i.e. 48% increase) for the granular layer with two geosynthetic layers (i.e. 2×1000 kN/m) which is shown in Fig. 6a. This is due to the accumulation of more loads on the LTP in the soft soil region for larger column spacing. Furthermore, since the area replacement ratio reduces as the spacing rises, the equivalent subgrade reaction of column decreases, and therefore the equivalent rigidity of the column supports also decreases, resulting in more settlement of LTP. Fig 6a also illustrates that the maximum settlement of the single layer geosynthetic reinforced LTP (i.e. 1×2000 kN/m) is higher than that of the double layer geosynthetic reinforced LTP (i.e. 2×1000 kN/m). For example, at $s/d = 3$, the maximum settlement of LTP with single geosynthetic reinforcement (i.e. 1×2000 kN/m) is 27 mm which decreases to 25 mm while the LTP is reinforced with double geosynthetic layers (i.e. 2×1000 kN/m). As Table 3 indicates that the bending stiffness of the LTP with the single geosynthetic layer is less than that of double layer geosynthetic reinforcement. As a result, settlement is higher for single layer case. Figs. 6b shows the influence of column spacing on tension of geosynthetic reinforcement. It is observed that tension increases with the increase in column spacing. For example, the maximum normalised tensions in the top and the bottom geosynthetic layers increase from 0.46 to 0.57 (i.e. 24% rise) and from 0.22 to 0.28 (i.e. 27% growth), respectively, as s/d increases from 3 to 3.5. Referring to Fig. 6a, it is obvious that as the settlement of LTP increases with the increasing column spacing, the axial strain of the geosynthetic reinforcement also increases causing more tension in the geosynthetic reinforcement. Abusharar et al. (2009) also observed similar trend during an empirical analysis of a pile supported embankment. Similar ranges of strains developed in the geosynthetics were reported by Rowe and Liu (2015) while a finite element modelling of a full-scale geosynthetic-reinforced, pile-supported embankment was presented. It can be seen that the change in the tensile force with column spacing for one geosynthetic reinforcement follows the similar trend as double layers' case reported in Fig. 6b. Furthermore, for s/d = 3, it is displayed that the one layer of geosynthetic reinforcement (i.e. 1×2000 kN/m) attracts 8% and 55% more normalised tension than the top and the bottom layer of geosynthetics, respectively in case of two layers geosynthetic reinforcement.

4.3. Effects of LTP thickness

As anticipated, increase in the LTP thickness results in the reduced maximum settlement of LTP which is displayed in Fig. 7a. For example, when the granular layer is reinforced with two geosynthetic layers (i.e. 2×1000 kN/m), the maximum settlement of LTP decreases 20% (i.e. from 25 mm to 20 mm) as the non-dimensional LTP thickness (h/d) increases from 1.5 to 1.75, which is presented in Fig. 7a. Parametric study reveals that as the thickness of LTP increases the equivalent bending stiffness and shear stiffness of LTP also increase. For example, as the non-dimensional thickness of LTP (h/d) increases from 1.5 to 1.75, the equivalent bending stiffness and shear stiffness of LTP with two geosynthetic layers (i.e. 2×1000 kN/m) increase by 33% and 14%, respectively. Thus, as the LTP becomes thicker, it becomes more inflexible which results in reduced settlement as visualised in Fig 7a. Referring to Fig 7a, the maximum settlement of LTP decreases when a single layer geosynthetic layer (i.e. 1×2000 kN/m) is replaced by two geosynthetics layers (i.e. 2×1000 kN/m). In addition, it is also noticed that this reduction in the maximum settlement is more noticeable for thinner LTP as compared to thicker LTP. For example, at the non-dimensional LTP thickness $h/d = 1.25$, 9% reduction in the maximum settlement of LTP is observed when a single layer of geosynthetic reinforcement (i.e.1×2000 kN/m) is replaced by two layers of geosynthetic reinforcement (i.e. 2×1000 kN/m) as shown in Fig. 7a. On the other hand, when the non-dimensional LTP thickness $h/d = 2$ is adopted, only 4% drop in the maximum settlement of LTP is perceived when a single layer of geosynthetic reinforcement (i.e. 1×2000 kN/m) is replaced by two layers of geosynthetic reinforcement (i.e. 2×1000 kN/m). The effect of LTP thickness on the maximum tension in the geosynthetic reinforcement is captured in Fig. 7b. This figure shows that the maximum mobilised tension in the geosynthetic reinforcement decreases with the thickness of LTP. The reason is that as LTP becomes thicker, it settles less (refer to Fig. 7a), and thus the axial strain of the geosynthetic reinforcement decreases, mobilising less tension in the geosynthetic reinforcement. As shown in Fig. 7b, for the granular layer with two geosynthetic layers (2×1000 kN/m), the maximum normalised mobilised tension in the top and the bottom geosynthetic layers are reduced by 13% and 9%, respectively when h/d increases from 1.5 to 1.75. It should be noted that similar trends occur for granular fill with a single geosynthetic layer (i.e. 1×2000 kN/m) in which the maximum mobilised tension in the geosynthetics is smaller with thicker LTP compared with thinner LTP which is shown in Fig. 7b.

4.4. *Effects of soft soil stiffness*

Effects of the soft soil stiffness on the maximum settlement of LTP are demonstrated in Fig. 8a. As evident in Fig. 8a, the maximum settlement of LTP decreases as the stiffness of soft soil increases. For example, the maximum deflection of LTP is reduced by 30% as elastic modulus of the soft soil (E_s) increases from 1000 kPa to 4000 kPa for LTP with double geosynthetics (i.e. 2×1000 kN/m). This can be explained by the fact that when soil is stiffer (i.e. soil with higher E_s value), the spring constants (k_u and k_l) and shear modulus (G) of the soil are also larger resulting in less deflection predictions for the soil. Hence, as the soil stiffness increases, the soft soil experiences less settlement, reflected in the LTP deformation. Obviously, similar relationship between the maximum deflection of LTP and the stiffness of the soft soil is observed when only one geosynthetic layer (i.e. 1×2000 kN/m) is adopted. Fig. 8b shows the effect of soft soil stiffness on mobilised tension in geosynthetic reinforcement. It is observed that as the stiffness of soft soil increases tension in geosynthetic reinforcement decreases. This is due to the fact that the increase in stiffness of soft soil causes less settlement of LTP and due to this reason less axial strain and tension are induced in the geosynthetic layer. For example, as the elastic modulus of the soft soil increases from 1000 kPa to 4000 kPa, the maximum normalised tension in the top and the bottom geosynthetic layers decreases from 0.46 to 0.3 (i.e. 35% reduction) and from 0.23 to 0.16 (i.e. 30% fall), respectively. A similar trend is observed for the case with single layer of geosynthetic as presented in Figs. 8b.

4.5. *Effects of tensile stiffness of geosynthetic reinforcement*

Fig. 9a displays the effect of tensile stiffness of geosynthetic reinforcement on the maximum settlement of LTP. As shown in Fig. 9a, the maximum settlement of LTP decreases as the tensile stiffness of geosynthetic reinforcement increases. For example, as the tensile stiffness of the each geosynthetic reinforcement for double layer case increases from 1000 kN/m to 2000 kN/m (i.e. from 2×1000 kN/m to 2×2000 kN/m), the maximum deflection of LTP decreases 24% (i.e. from 25 mm to 19 mm) which is plotted in Fig. 9a. This can be clarified by the point that as the tensile stiffness of geosynthetic reinforcement increases from 2×1000 kN/m to 2×2000 kN/m, the equivalent bending and shear stiffness of LTP becomes almost double (see Eqs. (2) and (3)) which results in less deflection of LTP. Similar patterns were also observed in the literature during the numerical analysis of a geosynthetic-reinforced embankments over soft foundation (Rowe and Li, 2005, Han et al., 2007). Referring to Fig. 9b, due to the increase in the tensile stiffness of geosynthetic reinforcement, the maximum normalised tension in the geosynthetic reinforcement decreases. For example, as the tensile stiffness of the each geosynthetic reinforcement increases from 1000 kN/m to 2000 kN/m for the case of double layer, the maximum normalised tension in the top layer decreases 50% (i.e. from 0.46 to 0.23) (see Fig. 9b). As the tensile stiffness of the geosynthetic reinforcement increases, the settlement of the LTP decreases (see Fig. 9a), and consequently the axial strain of the geosynthetic reinforcement decreases. Liu and Rowe (2015) also observed similar trend during a numerical analysis of a deep-mixing column supported embankment. However, the tension mobilised in the geosynthetic reinforcement increases. This increase in the mobilised tension is due to the fact that the mobilised tension is the product of the tensile stiffness and the axial strain of the geosynthetic layer (see Eqs. (39a) and (39b)). Therefore, as the tensile stiffness of the geosynthetic reinforcement increases the maximum mobilised tension also increases. Similar results were reported by Huang and Han (2010), and Bhasi and Rajagopal (2015) for geosynthetic reinforced embankments constructed on columns where numerical simulations were carried out. However, normalised tension is the ratio of mobilised tension in the geosynthetic (T) and ultimate strength (T_y) of the geosynthetics. It is observed that as the tensile stiffness of the geosynthetic reinforcement increases this ratio is decreased. Similar trends of the maximum deflections and normalised tensions are observed for the case with single layer of geosynthetic as presented in Figs. 9a−b.

It is mention worthy that the variations of deflection of LTP or tension in the geosynthetic reinforcement with the distance between two geosynthetic layers can be predicted using the proposed analytical solution in this study. It has been noticed that as the distance between two layers of geosynthetic reinforcements reduces, more deflection of LTP as well as the tension in geosynthetics are observed. Indeed, when the geosynthetic layers are positioned closely, the effective bending stiffness of the LTP (cracked LTP) is reduced contributing to more deflection of LTP and hence more tension in the geosynthetics. For example, for the baseline case, when the distance between two layers of geosynthetics is $2\,h/3$, the equivalent bending stiffness of LTP in sagging and hogging regions is equal to 263 kN.m. However, when the distance between two layers of geosynthetics is $h/3$, the equivalent bending stiffness of LTP in sagging and hogging regions is reduced to 161 kN.m. Therefore, deflection of LTP as well as mobilised tension in geosynthetics reinforcement increase as the spacing between geosynthetic layers decreases.

Indeed, in this paper a simple analytical model to predict the settlement behaviour of LTP on soft soil, reinforced by column inclusions such as unreinforced concrete columns and reinforced piles, has been presented. To achieve the objective of the paper, a closed-form solution has been developed to assess the performance of the load transfer platform for a general symmetric loading pattern. Therefore, the proposed model can be applied for any shape of symmetric loads from super structures such as embankments, silo, or fuel tanks where LTP over the columns is used. Indeed, since a general form of symmetric external loading has been adopted in this study (see Eq. (11)), user can adjust the model parameters to simulate different patterns of applied loading including those obtained from existing arching theories for embankments. It can be noted that a similar scenario of uniform loading was adopted by other researchers (Yin, 2000a, b; Zhang et al., 2012a; Borges and Gonçalves, 2016) to investigate the behaviour of load transfer platform on soft soil.Although, the loading due to arching can be symmetric close to middle of the embankments, but close to the batter or slopes, the loading due to arching would not be symmetric. The proposed model cannot be used for asymmetric loads such as arching below batters of embankments. Thus, this is one of the limitations of the proposed model.

5. Conclusions

The present study makes an attempt to suggest a reasonably accurate mechanical model for LTP reinforced with double layers of geosynthetics on column reinforced soft soil, which can be used by practicing engineers to investigate the flexural and shear behaviours of the LTP. The response function of the system has been derived for symmetric loading in plane strain conditions. This has been achieved by developing governing differential equations for the proposed model and its solutions. In order to develop analytical equations, the basic differential equations of a Timoshenko beam subjected to a distributed transverse load and a foundation interface pressure, generated from the Kerr foundation model were adopted. The homogeneous solution of the governing sixth order nonhomogeneous differential equation was found from the roots of the characteristic polynomial equation. Then adopting the method of Undetermined Coefficients, the particular solution was obtained. The proposed mechanical model can be beneficial for practicing engineers in analysing the settlement response of the multilayer geosynthetic reinforced granular bed overlying column improved soft soil.

Furthermore, soft soil idealised by the Winkler and the Pasternak foundations were used to evaluate the accuracy of the adopted Kerr foundation model to detail study of LTP on column improved soft soil. In general, the Winkler model produced higher values of displacements, rotations, bending moments, shear forces, and tensions than the reference solutions adopting the Kerr foundation model. However, the values of the displacements, rotations, bending moments, shear forces, and tensions obtained from Pasternak foundation model were smaller than the respective reference values adopting the Kerr foundation model. Kerr foundation model predicted the response of the soft soil more accurately, which were between two upper and lower bounds corresponding to the Winkler and the Pasternak foundation models. Therefore, it can be concluded that the Kerr foundation model is superior to the Winkler and the Pasternak models for the representation of the soil response. It should be noted that this theoretical model with its closed form solution may simulate the exact performance of the LTP under loading. However, the presented model can be used as a tool for a better estimation of the LTP behaviour with multi layers of geosynthetics, in comparison with the situation that soft soil is modelled by Winkler and Pasternak foundations.

Furthermore, using the proposed mechanical model, response of double layer geosynthetic reinforced LTP was compared with a single layer geosynthetic reinforced LTP. It was observed that inclusion of the two geosynthetic layers (i.e. 2×1000 kN/m) further reduced the maximum deflection of the LTP when compared to a single layer (i.e. 1×2000 kN/m). However, for the double layer case, the strength of geosynthetics was less utilised than that of the single layer case. It was also revealed that in the double layer reinforcement, the top geosynthetic layer was more effective at the column location (in the hogging region), whereas the bottom geosynthetic layer was more effective in the middle span (in the sagging region). It was also noticed that top geosynthetic layer was subjected to higher mobilised tension than the bottom layer. Moreover, it can be concluded that the use of one stronger geosynthetic layer (e.g. 1×2000 kN/m) with the equivalent stiffness of two geosynthetic layers (e.g. 2×1000 kN/m), does not result in the same settlement of LTP and the tension of the geosynthetic reinforcement when compared to two weaker geosynthetic layers (e.g. 2×1000 kN/m).

Acknowledgement

The first author acknowledges the financial support received from Roads and Maritime Services (RMS), SMEC Australia, Fulton Hogan, and Menard-Oceania. The authors wish to thank A. H. M. Kamruzzaman from Roads and Maritime Services (RMS) for his valuable comments at different stages of the project.

Appendix:

Summary of thirteen algebraic equations obtained from the adopted boundary and continuity conditions

According to the boundary condition $V_s^{LTP} = 0$, the following equation is obtained:

$$c_1K_1 - c_2K_1 + c_3L_1 - c_4M_1 - c_5L_1 - c_6M_1 = R_1 \tag{51}$$

Boundary condition $w_s^{LTP'} = 0$ results:

$$c_1\delta_s - c_2\delta_s + c_3\varepsilon_s - c_4\sigma_s - c_5\varepsilon_s - c_6\sigma_s = R_2 \tag{52}$$

From the boundary condition $V_h^{LTP} = -(K_c)_{eq}w_h^{LTP}$ following equation is obtained:

$$\begin{aligned} &-d_1e^{-\left(\frac{\delta_h s}{2}\right)}A_{22} + d_2e^{\left(\frac{\delta_h s}{2}\right)}B_{22} - d_3e^{-\left(\frac{\varepsilon_h s}{2}\right)}\left[C_{22}\sin\left(\frac{\sigma_h s}{2}\right) + E_{22}\cos\left(\frac{\sigma_h s}{2}\right)\right] - d_4e^{-\left(\frac{\varepsilon_h s}{2}\right)}\left[E_{22}\sin\left(\frac{\sigma_h s}{2}\right) - C_{22}\cos\left(\frac{\sigma_h s}{2}\right)\right] - \\ &d_5e^{\left(\frac{\varepsilon_h s}{2}\right)}\left[C_{22}\sin\left(\frac{\sigma_h s}{2}\right) - D_{22}\cos\left(\frac{\sigma_h s}{2}\right)\right] + d_6e^{\left(\frac{\varepsilon_h s}{2}\right)}\left[D_{22}\sin\left(\frac{\sigma_h s}{2}\right) + C_{22}\cos\left(\frac{\sigma_h s}{2}\right)\right] = R_3 \end{aligned} \tag{53}$$

Assuming

$$A_{22} = K_2C - (K_c)_{eq};\ B_{22} = K_2C + (K_c)_{eq}\ ;\ C_{22} = CM_2\ ;\ D_{22} = CL_2 + (K_c)_{eq}\ ;\ \text{and}\ E_{22} = CL_2 - (K_c)_{eq} \tag{54}$$

The equation below is obtained from the boundary condition $\theta_h^{LTP} = 0$:

$$-d_1 e^{-\left(\frac{\delta_h s}{2}\right)} A_2 + d_2 e^{\left(\frac{\delta_h s}{2}\right)} A_2 - d_3 e^{-\left(\frac{\varepsilon_h s}{2}\right)} \left[B_2 \sin\left(\frac{\sigma_h s}{2}\right) - C_2 \cos\left(\frac{\sigma_h s}{2}\right)\right] + d_4 e^{-\left(\frac{\varepsilon_h s}{2}\right)} \left[C_2 \sin\left(\frac{\sigma_h s}{2}\right) + B_2 \cos\left(\frac{\sigma_h s}{2}\right)\right] -$$

$$d_5 e^{\left(\frac{\varepsilon_h s}{2}\right)} \left[B_2 \sin\left(\frac{\sigma_h s}{2}\right) + C_2 \cos\left(\frac{\sigma_h s}{2}\right)\right] - d_6 e^{\left(\frac{\varepsilon_h s}{2}\right)} \left[C_2 \sin\left(\frac{\sigma_h s}{2}\right) - B_2 \cos\left(\frac{\sigma_h s}{2}\right)\right] = R_4 \tag{55}$$

1000 From the boundary condition $w_s^{LTP} = w_h^{LTP}$ the following equation is obtained:

$$-c_1 e^{-\delta_s r} - c_2 e^{\delta_s r} - c_3 e^{-\varepsilon_s r} \cos\sigma_s r - c_4 e^{-\varepsilon_s r} \sin\sigma_s r - c_5 e^{\varepsilon_s r} \cos\sigma_s r - c_6 e^{\varepsilon_s r} \sin\sigma_s r + d_1 e^{-\delta_h r} + d_2 e^{\delta_h r} + d_3 e^{-\varepsilon_h r} \cos\sigma_h r +$$

$$d_4 e^{-\varepsilon_h r} \sin\sigma_h r + d_5 e^{\varepsilon_h r} \cos\sigma_h r + d_6 e^{\varepsilon_h r} \sin\sigma_h r = R_5 \tag{56}$$

1001 According to the boundary condition $\theta_s^{LTP} = \theta_h^{LTP}$ the following equation is obtained:

$$c_1 e^{-\delta_s r} A_1 - c_2 e^{\delta_s r} A_1 + c_3 e^{-\varepsilon_s r}(B_1 \sin\sigma_s r - C_1 \cos\sigma_s r) - c_4 e^{-\varepsilon_s r}(C_1 \sin\sigma_s r + B_1 \cos\sigma_s r) + c_5 e^{\varepsilon_s r}(B_1 \sin\sigma_s r + C_1 \cos\sigma_s r) +$$

$$c_6 e^{\varepsilon_s r}(C_1 \sin\sigma_s r - B_1 \cos\sigma_s r) - d_1 e^{-\delta_h r} A_2 + d_2 e^{\delta_h r} A_2 - d_3 e^{-\varepsilon_h r}(B_2 \sin\sigma_h r - C_2 \cos\sigma_h r) + d_4 e^{-\varepsilon_h r}(C_2 \sin\sigma_h r +$$

$$B_2 \cos\sigma_h r) - d_5 e^{\varepsilon_h r}(B_2 \sin\sigma_h r + C_2 \cos\sigma_h r) - d_6 e^{\varepsilon_h r}(C_2 \sin\sigma_h r - B_2 \cos\sigma_h r) = R_6 \tag{57}$$

1002 The following equation is after $M_h^{LTP} = 0$:

$$d_1 e^{-\delta_h r} \delta_h A_2 + d_2 e^{\delta_h r} \delta_h A_2 + d_3 e^{-\varepsilon_h r}(J_2 \sin\sigma_h r - I_2 \cos\sigma_h r) - d_4 e^{-\varepsilon_h r}(I_2 \sin\sigma_h r + J_2 \cos\sigma_h r) - d_5 e^{\varepsilon_h r}(J_2 \sin\sigma_h r +$$

$$I_2 \cos\sigma_h r) - d_6 e^{\varepsilon_h r}(I_2 \sin\sigma_h r - J_2 \cos\sigma_h r) = R_7 \tag{58}$$

1003 The following equation is obtained from $V_s^{LTP} = V_h^{LTP}$:

$$-c_1e^{-\delta_s r}K_1C + c_2e^{\delta_s r}K_1C - c_3e^{-\varepsilon_s r}C(M_1\sin\sigma_s r + L_1\cos\sigma_s r) - c_4e^{-\varepsilon_s r}C(L_1\sin\sigma_s r - M_1\cos\sigma_s r) - c_5e^{\varepsilon_s r}C(M_1\sin\sigma_s r - L_1\cos\sigma_s r) + c_6e^{\varepsilon_s r}C(L_1\sin\sigma_s r + M_1\cos\sigma_s r) + d_1e^{-\delta_h r}K_2C - d_2e^{\delta_h r}K_2C + d_3e^{-\varepsilon_h r}C(M_2\sin\sigma_h r + L_2\cos\sigma_h r) + d_4e^{-\varepsilon_h r}C(L_2\sin\sigma_h r - M_2\cos\sigma_h r) + d_5e^{\varepsilon_h r}C(M_2\sin\sigma_h r - L_2\cos\sigma_h r) - d_6e^{\varepsilon_h r}C(L_2\sin\sigma_h r + M_2\cos\sigma_h r) = R_8 \quad (59)$$

1004 The next equation is obtained using $M_s^{LTP} = 0$:

$$c_1e^{-\delta_s r}\delta_sA_1 + c_2e^{\delta_s r}\delta_sA_1 + c_3e^{-\varepsilon_s r}(J_1\sin\sigma_s r - I_1\cos\sigma_s r) - c_4e^{-\varepsilon_s r}(I_1\sin\sigma_s r + J_1\cos\sigma_s r) - c_5e^{\varepsilon_s r}(J_1\sin\sigma_s r + I_1\cos\sigma_s r) - c_6e^{\varepsilon_s r}(I_1\sin\sigma_s r - J_1\cos\sigma_s r) = R_9 \quad (60)$$

1005 The equation below is obtained from $V_h^{ls} = (K_c)_{eq}\left(\frac{G}{C}\right)w_h^{ls}$:

$$d_1e^{-\left(\frac{\delta_h s}{2}\right)}L_{22} - d_2e^{\left(\frac{\delta_h s}{2}\right)}L_{22} + d_3e^{-\left(\frac{\varepsilon_h s}{2}\right)}\left[M_{22}\cos\left(\frac{\sigma_h s}{2}\right) - N_{22}\sin\left(\frac{\sigma_h s}{2}\right)\right] + d_4e^{-\left(\frac{\varepsilon_h s}{2}\right)}\left[N_{22}\cos\left(\frac{\sigma_h s}{2}\right) + M_{22}\sin\left(\frac{\sigma_h s}{2}\right)\right] - d_5e^{\left(\frac{\varepsilon_h s}{2}\right)}\left[M_{22}\cos\left(\frac{\sigma_h s}{2}\right) + M_{22}\sin\left(\frac{\sigma_h s}{2}\right)\right] + d_6e^{\left(\frac{\varepsilon_h s}{2}\right)}\left[N_{22}\cos\left(\frac{\sigma_h s}{2}\right) - M_{22}\sin\left(\frac{\sigma_h s}{2}\right)\right] = R_{10} \quad (61)$$

1006 Assuming

$L_{22} = -\delta_h\left\{{\delta_h}^4U_2 - \frac{{\delta_h}^2U_2k_u}{C} + Y_2\right\}$; $M_{22} = -({\varepsilon_h}^5 - 10{\varepsilon_h}^3{\sigma_h}^2 + 5\varepsilon_h{\sigma_h}^4)U_2 + ({\varepsilon_h}^3 - 3\varepsilon_h{\sigma_h}^2)\frac{U_2k_u}{C} - Y_2\varepsilon_h$; and

$$N_{22} = (5{\varepsilon_h}^4\sigma_h - 10{\varepsilon_h}^2{\sigma_h}^3 + {\sigma_h}^5)U_2 - (3{\varepsilon_h}^2\sigma_h - {\sigma_h}^3)\frac{U_2k_u}{C} + Y_2\sigma_h \quad (62)$$

1007 The following equation is obtained from $w_s^{ls\prime} = 0$:

$$c_1L_{11} - c_2L_{11} + c_3M_{11} + c_4N_{11} - c_5M_{11} + c_6N_{11} = R_{11} \tag{63}$$

Assuming

$$L_{11} = -\delta_s\left(\delta_s{}^4U_1 - \frac{U_1k_u\delta_s{}^2}{C} + Y_1\right);\ M_{11} = -(\varepsilon_s{}^5 - 10\varepsilon_s{}^3\sigma_s{}^2 + 5\varepsilon_s\sigma_s{}^4)U_1 + (\varepsilon_s{}^3 - 3\varepsilon_s\sigma_s{}^2)\frac{U_1k_u}{C} - Y_1\varepsilon_s\ ;\text{ and}$$

$$N_{11} = (5\varepsilon_s{}^4\sigma_s - 10\varepsilon_s{}^2\sigma_s{}^3 + \sigma_s{}^5)U_1 - (3\varepsilon_s{}^2\sigma_s - \sigma_s{}^3)\frac{U_1k_u}{C} + \sigma_sY_1 \tag{64}$$

The equation below is obtained using $w_s^{ls} = w_h^{ls}$:

$$c_1e^{-\delta_sr}F_{11} + c_2e^{\delta_sr}F_{11} + c_3e^{-\varepsilon_sr}(G_{11}\sin\sigma_sr + H_{11}\cos\sigma_sr) + c_4e^{-\varepsilon_sr}(H_{11}\sin\sigma_sr - G_{11}\cos\sigma_sr) - c_5e^{\varepsilon_1r}(G_{11}\sin\sigma_sr - H_{11}\cos\sigma_sr) + c_6e^{\varepsilon_sr}(H_{11}\sin\sigma_sr + G_{11}\cos\sigma_sr) - d_1e^{-\delta_hr}F_{22} - d_2e^{\delta_hr}F_{22} - d_3e^{-\varepsilon_hr}(G_{22}\sin\sigma_hr + H_{22}\cos\sigma_hr) - d_4e^{-\varepsilon_hr}(H_{22}\sin\sigma_hr - G_{22}\cos\sigma_hr) + d_5e^{\varepsilon_hr}(G_{22}\sin\sigma_hr - H_{22}\cos\sigma_hr) - d_6e^{\varepsilon_hr}(H_{22}\sin\sigma_hr + G_{22}\cos\sigma_hr) = R_{12} \tag{65}$$

Assuming

$$G_{11} = U_1(4\varepsilon_s{}^3\sigma_s - 4\varepsilon_s\sigma_s{}^3) - \frac{U_1k_u}{C}(2\varepsilon_s\sigma_s);\ H_{11} = U_1(\varepsilon_s{}^4 - 6\varepsilon_s{}^2\sigma_s{}^2 + \sigma_s{}^4) - \frac{U_1k_u}{C}(\varepsilon_s{}^2 - \sigma_s{}^2) + Y_1;\ F_{11} = \delta_s{}^4U_1 - \delta_s{}^2\frac{Q_1k_u}{C} + Y_1;$$

$$G_{22} = U_2(4\varepsilon_h{}^3\sigma_h - 4\varepsilon_h\sigma_h{}^3) - \frac{U_2k_u}{C}(2\varepsilon_h\sigma_h)\ ;\ H_{22} = U_2(\varepsilon_h{}^4 - 6\varepsilon_h{}^2\sigma_h{}^2 + \sigma_h{}^4) - \frac{U_2k_u}{C}(\varepsilon_h{}^2 - \sigma_h{}^2) + Y_2\ ;\ F_{22} = \delta_h{}^4U_2 - \delta_h{}^2\frac{U_2k_u}{C} + \tag{66}$$

The following equation is obtained from $w_s^{ls'} = w_h^{ls'}$:

$$c_1 e^{-\delta_s r} L_{11} - c_2 e^{\delta_s r} L_{11} + c_3 e^{-\varepsilon_s r}(M_{11}\cos\sigma_s r - N_{11}\sin\sigma_s r) + c_4 e^{-\varepsilon_s r}(N_{11}\cos\sigma_s r + M_{11}\sin\sigma_s r) - c_5 e^{\varepsilon_s r}(M_{11}\cos\sigma_s r + N_{11}\sin\sigma_s r) + e^{\varepsilon_s r} c_6 (N_{11}\cos\sigma_s r - M_{11}\sin\sigma_s r) - d_1 e^{-\delta_h r} L_{22} + d_2 e^{\delta_h r} L_{22} - d_3 e^{-\varepsilon_h r}(M_{22}\cos\sigma_h r - N_{22}\sin\sigma_h r) - d_4 e^{-\varepsilon_h r}(N_{22}\cos\sigma_h r + M_{22}\sin\sigma_h r) + d_5 e^{\varepsilon_h r}(M_{22}\cos\sigma_h r + N_{22}\sin\sigma_h r) - d_6 e^{\varepsilon_h r}(N_{22}\cos\sigma_h r - M_{22}\sin\sigma_h r) = R_{13} \qquad (67)$$

where

$$R_1 = 0 \qquad (68)$$

$$R_2 = 0 \qquad (69)$$

$$R_3 = -P_0 (K_c)_{eq} \frac{(k_u + k_l)}{k_u k_l} - C \sum_{n=1}^{n=\infty} \left\{ \left[D_2 + E_2 \left(\frac{2n\pi}{s}\right)^4 - F_2 \left(\frac{2n\pi}{s}\right)^2 - 1 \right] p_{nh} \right\} \left(\frac{2n\pi}{s}\right) \sin n\pi - \sum_{n=1}^{n=\infty} (K_c)_{eq} p_{nh} \cos n\pi \qquad (70)$$

$$R_4 = \sum_{n=1}^{n=\infty} \left\{ \left[D_2 + E_2 \left(\frac{2n\pi}{s}\right)^4 - F_2 \left(\frac{2n\pi}{s}\right)^2 \right] p_{nh} + \left[\left(\frac{GF_2 {D_s}^2}{C^2}\right) \left(\frac{2n\pi}{s}\right)^2 + \left[\left(\frac{GF_2 D_s}{C}\right) + \frac{D_s}{C^2} \right] \right] P_n \right\} \left(\frac{2n\pi}{s}\right) \sin n\pi \qquad (71)$$

$$R_5 = \sum_{n=1}^{n=\infty} \left[(p_{nh} - p_{ns}) \cos\left(\frac{2n\pi r}{s}\right) \right] \qquad (72)$$

$$R_6 = \sum_{n=1}^{n=\infty} \left\{ \left[D_1 + E_1 \left(\frac{2n\pi}{s}\right)^4 - F_1 \left(\frac{2n\pi}{s}\right)^2 \right] p_{ns} + \left[\left(\frac{GF_1 {D_s}^2}{C^2}\right) \left(\frac{2n\pi}{s}\right)^2 + \left[\left(\frac{GF_1 D_s}{C}\right) + \frac{D_s}{C^2} \right] \right] P_n \right\} \left(\frac{2n\pi}{s}\right) \sin\left(\frac{2n\pi r}{s}\right) - \sum_{n=1}^{n=\infty} \left\{ \left[D_2 + E_2 \left(\frac{2n\pi}{s}\right)^4 - F_2 \left(\frac{2n\pi}{s}\right)^2 \right] p_{nh} + \left[\left(\frac{GF_2 {D_h}^2}{C^2}\right) \left(\frac{2n\pi}{s}\right)^2 + \left[\left(\frac{GF_2 D_h}{C}\right) + \frac{D_h}{C^2} \right] \right] P_n \right\} \left(\frac{2n\pi}{s}\right) \sin\left(\frac{2n\pi r}{s}\right) \qquad (73)$$

$$R_7 = \sum_{n=1}^{n=\infty} \left\{\left[D_1 + E_1\left(\frac{2n\pi}{s}\right)^4 - F_1\left(\frac{2n\pi}{s}\right)^2\right]p_{ns} + \left[\left(\frac{GF_1{D_s}^2}{C^2}\right)\left(\frac{2n\pi}{s}\right)^2 + \left[\left(\frac{GF_1D_s}{C}\right) + \frac{D_s}{C^2}\right]\right]P_n\right\}\left(\frac{2n\pi}{s}\right)^2 \cos\left(\frac{2n\pi r}{s}\right) \tag{74}$$

$$R_8 = -C\sum_{n=1}^{n=\infty} \left\{\left[D_1 + E_1\left(\frac{2n\pi}{s}\right)^4 - F_1\left(\frac{2n\pi}{s}\right)^2 - 1\right]p_{ns} + \left[\left(\frac{GF_1{D_s}^2}{C^2}\right)\left(\frac{2n\pi}{s}\right)^2 + \left[\left(\frac{GF_1D_s}{C}\right) + \frac{D_s}{C^2}\right]\right]P_n\right\}\left(\frac{2n\pi}{s}\right) \sin\left(\frac{2n\pi r}{s}\right) +$$

$$C\sum_{n=1}^{n=\infty} \left\{\left[D_1 + E_1\left(\frac{2n\pi}{s}\right)^4 - F_1\left(\frac{2n\pi}{s}\right)^2 - 1\right]p_{nh} + \left[\left(\frac{GF_1{D_h}^2}{C^2}\right)\left(\frac{2n\pi}{s}\right)^2 + \left[\left(\frac{GF_1D_h}{C}\right) + \frac{D_h}{C^2}\right]\right]P_n\right\}\left(\frac{2n\pi}{s}\right) \sin\left(\frac{2n\pi r}{s}\right) \tag{75}$$

$$R_9 = \sum_{n=1}^{n=\infty} \left\{\left[D_2 + E_2\left(\frac{2n\pi}{s}\right)^4 - F_2\left(\frac{2n\pi}{s}\right)^2\right]p_{nh} + \left[\left(\frac{GF_2{D_h}^2}{C^2}\right)\left(\frac{2n\pi}{s}\right)^2 + \left[\left(\frac{GF_2D_h}{C}\right) + \frac{D_h}{C^2}\right]\right]P_n\right\}\left(\frac{2n\pi}{s}\right)^2 \cos\left(\frac{2n\pi r}{s}\right) \tag{76}$$

$$R_{10} = \frac{(K_c)_{eq}P_n}{C}\left[Z_2\left(\frac{k_u + k_l}{k_u k_l}\right) - \left(\frac{(K_c)_{eq}}{C}\right)\left(\frac{U_2}{D_h}\right)\right]P_0 - \sum_{n=1}^{n=\infty}\left\{\left[\left(\frac{U_2}{D_h}\right) + \left(\frac{U_2}{C}\right)\left(\frac{2n\pi}{s}\right)^2\right] + \left[V_2\left(\frac{2n\pi}{s}\right)^4 + X_2\left(\frac{2n\pi}{s}\right)^2 + Z_2\right]p_{nh}\right\}\cos n\pi -$$

$$\sum_{n=1}^{n=\infty}\left\{\left[\left(\frac{U_2}{D_h}\right) - \left(\frac{U_2}{C}\right)\left(\frac{2n\pi}{s}\right)^2\right]\left(\frac{2n\pi}{s}\right)P_n - \left[U_2\left(\frac{2n\pi}{s}\right)^4 + W_2\left(\frac{2n\pi}{s}\right)^2 + Y_2\right]\left(\frac{2n\pi}{s}\right)p_{nh}\right\}\sin n\pi \tag{77}$$

$$R_{11} = \sum_{n=1}^{n=\infty}\frac{U_1}{C}\left(\frac{2n\pi}{s}\right)^3 P_n \tag{78}$$

$$R_{12} = \left[\frac{(k_1+k_2)(Y_2-Y_1)}{k_1} + \left(\frac{U_1}{D_s} - \frac{U_2}{D_h}\right)\right]P_0 + \sum_{n=1}^{n=\infty}\left[\left(\frac{U_1}{D_s} - \frac{U_2}{D_h}\right) - \left(\frac{U_1}{C} - \frac{U_2}{C}\right)\left(\frac{2n\pi}{s}\right)^2\right]P_n\cos\left(\frac{2n\pi r}{s}\right) - \sum_{n=1}^{n=\infty}\left[\left(1 + \frac{U_1{k_u}^2}{CG}\right) - \left(\frac{U_1k_u}{C}\right)\left(\frac{2n\pi}{s}\right)^2 +\right.$$

$$\left.U_1\left(\frac{2n\pi}{s}\right)^4\right]p_{ns}\cos\left(\frac{2n\pi r}{s}\right) + \sum_{n=1}^{n=\infty}\left[\left(1 + \frac{U_2{k_u}^2}{CG}\right) + \left(\frac{U_2k_u}{C}\right)\left(\frac{2n\pi}{s}\right)^2 + U_2\left(\frac{2n\pi}{s}\right)^4\right]p_{nh}\cos\left(\frac{2n\pi r}{s}\right) \tag{79}$$

and

$$\mathrm{R}_{13} = \sum_{n=1}^{n=\infty}\left[\left(\frac{U_2}{C} - \frac{\mathrm{U}_1}{\mathrm{C}}\right)\left(\frac{2n\pi}{s}\right)^2 - \left(\frac{U_1}{D_s} + \frac{U_2}{D_h}\right)\right]\left(\frac{2n\pi}{s}\right)P_n \sin\left(\frac{2n\pi r}{s}\right) + \sum_{\mathrm{n}=1}^{\mathrm{n}=\infty}\left[U_1\left(\frac{2n\pi}{s}\right)^4 + W_1\left(\frac{2n\pi}{s}\right)^2 + Y_1\right]\left(\frac{2n\pi}{s}\right)p_{ns} \sin\left(\frac{2n\pi r}{s}\right) - \sum_{\mathrm{n}=1}^{\mathrm{n}=\infty}\left[U_2\left(\frac{2n\pi}{s}\right)^4 + W_2\left(\frac{2n\pi}{s}\right)^2 + Y_2\right]\left(\frac{2n\pi}{s}\right)p_{nh} \sin\left(\frac{2n\pi r}{s}\right) \quad (80)$$

Assuming

$$W_1 = \frac{U_1 k_u}{C};\ Y_1 = \frac{U_1 k_u k_l}{CG} + 1;\ W_2 = \frac{U_2 k_u}{C};\ Y_2 = \frac{U_2 k_u k_l}{CG} + 1;\ X_2 = \frac{(K_c)_{eq} U_2 k_u}{C^2};\ \text{and } Z_2 = \left(\frac{(K_c)_{eq}}{C}\right)\left(\frac{U_2 k_u k_l}{CG} + 1\right) \quad (81)$$

References

Abusharar, S.W., Zheng, J.J., Chen, B.G., Yin, J.H., 2009. A simplified method for analysis of a piled embankment reinforced with geosynthetics. Geotextiles and Geomembranes. 27 (1), 39–52.

Avramidis, I.E., Morfidis, K., 2006. Bending of beams on three-parameter elastic foundation. International Journal of Solids and Structures. 43 (2), 357–375.

Bergado, D., Ruenkrairergsa, T., Taesiriy, T.Y, Balasubramaniam, A.S., 1999. Deep soil mixing used to reduce embankment settlement. Ground Improvement. 3, 145–162.

Bhasi, A., Rajagopal, K., 2015. Geosynthetic-reinforced piled embankments: comparison of numerical and analytical methods. International Journal of Geomechanics. 15 (5), 1–12.

Borges, J.L., Gonçalves, M.S., 2016. Jet-grout column-reinforced soft soils incorporating multilayer geosynthetic-reinforced platforms. Soils and Foundations. 56 (1), 57–72.

Briançon, L., Simon, B., 2012. Performance of pile-supported embankment over soft soil: Full-scale experiment. Journal of Geotechnical and Geoenvironmental Engineering. 134 (4), 551–562.

BS8006-1, 2010. Code of practice for strengthened reinforced soils and other fills. British Standards Institution.

Carlsson, B., 1987. Reinforced Soil, Principles for Calculation. Terratema AB, Linköping (in Swedish).

Chen, R.P., Xu, Z.Z., Chen, Y.M., Ling, D.S., Zhu, B., 2010. Field test on a piled embankment over soft ground. Journal of Geotechnical and Geoenvironmental Engineering. 136 (6), 777–785.

Chen, Y.M., Cao, W.P., Chen, R.P., 2008. An experimental investigation of soil arching within basal reinforced and unreinforced piled embankments. Geotextiles and Geomembranes. 26 (2), 164–174.

Collin, J.G., Watson, C.H., Han, J., 2005. Column-supported embankment solves time constraint for new road construction. Foundation Engineering.

Cowper, G., 1966. The shear coefficient in Timoshenko's beam theory. Journal of applied mechanics. 33 (2), 335–340.

Deb, K., Basudhar, P.K., Chandra, S., 2007. Generalized model for geosynthetic-reinforced granular fill-soft soil with stone columns. International Journal of Geomechanics. 7 (4), 266–276.

Deb, K., 2010. A mathematical model to study the soil arching effect in stone column-supported embankment resting on soft foundation soil. Applied Mathematical Modelling. 34 (12), 3871–3883.

Deb, K., Mohapatra, S.R., 2013. Analysis of stone column-supported geosynthetic-reinforced embankments. Applied Mathematical Modelling. 37 (5), 2943–2960.

EBGEO, 2010. Empfehlungen für den Entwurf und die Berechnung von Erdkörpern mit Bewehrungen aus Geokunststoffen German Geotechnical Society 2.

Farag, G.S.F., 2008. Lateral spreading in basal reinforced embankments supported by pile-like elements. In: Schiftenreihe Getechnik. Universität Kassel. Heft 20.

Filonenko-Borodich, M.M., 1940. Some approximate theories of the elastic foundation. Uchenyie Zapiski Moskovskogo Gosudarstvennogo Universiteta Mekhanica 46, 3–18.

Filz, G.M., Smith, M.E., 2007. Net Vertical Loads on Geosynthetic Reinforcement in Column-Supported Embankments. Soil Improvement GSP 172. 1–10.

Filz, G., Sloan, J., McGuire, M.P., Collin, J., Smith, M., 2012. Column-supported embankments: Settlement and load transfer. In: Proceedings of Geo–Congress, Oakland, California.

Ghosh, B., Fatahi, B., Khabbaz, H., 2016. Analytical solution to analyze LTP on column-improved soft soil considering soil nonlinearity. International Journal of Geomechanics. 04016082, 1–24.

Girout, R., Blanc, M., Thorel, L., Fagundes, D.F., Almeida, M.S.S., 2016. Arching and Deformation in a Piled Embankment: Centrifuge Tests Compared to Analytical Calculations. Journal of Geotechnical and Geoenvironmental Engineering. 142 (12).

Gray, H., 1944. Simultaneous consolidation of contiguous layers of unlike compressible soils. Proceedings of the American Society of Civil Engineers, ASCE.

Han, J., 2001. Simplified method for consolidation rate of stone column reinforced foundations. Journal of Geotechnical and Geoenvironmental Engineering. 127 (7), 597-603.

Han, J., Gabr, M.A., 2002. Numerical analysis of geosynthetic-reinforced and pile-supported earth platforms over soft soil. Journal of Geotechnical and Geoenvironmental Engineering. 128 (1), 44–53.

Han, J., Collin, J.G., Huang, J., 2004. Recent development of geosynthetic-reinforced column-supported embankments. The 55th Highway Geology Symposium. Kansas City, Missouri: 299–321.

Han, J., Oztoprak, S., Parsons, R.L., Huang, J., 2007. Numerical analysis of foundation columns to support widening of embankments. Computers and Geotechnics. 34 (6), 435–448.

Heitz, C., 2006. Bodengewölbe unter ruhender und nichtruhender Belastung bei Berücksichtigung von Bewehrungseinlagen aus Geogittern. In: Schriftenreihe Geotechnik. Uni Kassel. Heft 19, November 2006 (in German).

Hetényi, M., 1946. Beams on elastic foundation: Theory with applications in the fields of civil and mechanical engineering, University of Michigan Press.

Hewlett, W., Randolph, M.A., 1988. Analysis of piled embankments. Ground Engineering. 21 (3), 12–18.

Horvath, J.S., 1983. Modulus of subgrade reaction: New perspective. Journal of Geotechnical Engineering. 109 (12), 1591–1596.

Huang, J., Han, J., 2009. 3D coupled mechanical and hydraulic modeling of a geosynthetic-reinforced deep mixed column-supported embankment. Geotextiles and Geomembranes. 27 (4), 272–280.

Huang, J., Han, J., Oztoprak, S., 2009. Coupled mechanical and hydraulic modeling of geosynthetic-reinforced column-supported embankments. Journal of Geotechnical and Geoenvironmental Engineering. 135 (8), 1011–1021.

Huang, J., Han, J., 2010. Two-dimensional parametric study of geosynthetic-reinforced column-supported embankments by coupled hydraulic and mechanical modeling. Computers and Geotechnics. 37 (5), 638–648.

Hutchinson, J.R., 2001. Shear coefficients for Timoshenko beam theory. Journal of Applied Mechanics. 68 (1), 87.

Indraratna, B., Rujikiatkamjorn, C., Sathananthan, I., 2005. Radial consolidation of clay using compressibility indices and varying horizontal permeability. Canadian Geotechinical Journal. 42, 1330–1341.

Indraratna, B., Basack, S., Rujikiatkamjorn, C., 2013a. Numerical solution of stone column–improved soft soil considering arching, clogging, and smear effects. Journal of Geotechnical and Geoenvironmental Engineering. 139 (3), 377–394.

Indraratna, B., Ngo, N.T., Rujikiatkamjorn, C., 2013b. Deformation of coal fouled ballast stabilized with geogrid under cyclic load. Journal of Geotechnical and Geoenvironmental Engineering. 139 (8), 1275–1289.

Jones, C.J.F.P., Lawson, C.R., Ayres, D.J., 1990. Geotextile reinforced piled embankments. In: Hoedt, Den (Ed.), Geotextiles, Geomembranes and Related Products, Balkema, Rotterdam.

Jones, R., Xenophontos, J., 1976. On the Vlasov and Kerr foundation models. Acta Mechanica 25, 45–49.

Kempfert, H.G., Göbel, C., Alexiew, D., Heitz, C., 2004. German recommendations for reinforced embankments on pile-similar elements. In: Proceedings of EuroGeo 3, Munich.

Kerr, A.D., 1964. Elastic and viscoelastic foundation models. Journal of Applied Mechanics. 31 (3), 491–498.

Kerr, A.D., 1965. A study of a new foundation model. Acta Mechanica 1, 135–147.

Khabbazian, M., Kaliakin, V.N., Meehan, C.L., 2015. Column Supported Embankments with Geosynthetic Encased Columns: Validity of the Unit Cell Concept. Geotechnical and Geological Engineering. 33 (3), 425–442.

Kneifati, M.C., 1985. Analysis of plates on a Kerr foundation model. Journal of Engineering Mechanics. 111 (11), 1325–1342.

Lei, G.H., Fu, C.W., Ng, C.W.W., 2016. Vertical-drain consolidation using stone columns: An analytical solution with an impeded drainage boundary under multi-ramp loading. Geotextiles and Geomembranes. 44 (1), 122–131.

Liu, H.L., Ng, C.W.W., Fei, K., 2007. Performance of a geogrid-reinforced and pile-supported highway embankment over soft clay: Case study. Journal of Geotechnical and Geoenvironmental Engineering. 133 (12), 1483–1493.

Liu, H., Kong, G., Chu, J., Ding, X., 2015. Grouted gravel column-supported highway embankment over soft clay: case study. Canadian Geotechnical Journal. 52 (11), 1725–1733.

Liu, K.W., Rowe, R.K., 2015. Numerical study of the effects of geosynthetic reinforcement viscosity on behaviour of embankments supported by deep-mixing-method columns. Geotextiles and Geomembranes. 43 (6), 567–578.

Low, B.K., Tang, S.K., Choa, V., 1994. Arching in piled embankments. Journal of Geotechical Engineering. 120 (11), 1917–1938.

Maheshwari, P., Basudhar, P., Chandra, S., 2004. Analysis of beams on reinforced granular beds. Geosynthetics International. 11 (6), 470–480.

Maheshwari, P., Viladkar, M.N., 2009. A mathematical model for beams on geosynthetic reinforced earth beds under strip loading. Applied Mathematical Modelling. 33 (4), 1803–1814.

Marston, A., Anderson, A.O., 1913. The theory of loads on pipes in ditches: and tests of cement and clay drain tile and sewer pipe, Iowa State College of Agriculture and Mechanic Arts.

MathWorks, MATLAB R2016b Optimization Toolbox™ User's Guide. U.S.A.

McGuire, M., Sloan, J., Collin, J., Filz, G., 2012. Critical height of column-supported embankments from Bench-Scale and field-scale tests. In: TC 211 International Symposium on Ground Improvement IS-GI Brussels, ISSMGE.

McKelvey, J.A., 1994. The anatomy of soil arching. Geotextiles and Geomembranes. 13 (5), 317–329.

Morfidis, K., 2007. Exact matrices for beams on three-parameter elastic foundation. Computers and Structures. 85 (15–16), 1243–1256.

Naughton, P., 2007. The significance of critical height in the design of piled embankments. Soil Improvement, 1–10.

Nogami, T., Yong, T.Y., 2003. Load-settlement analysis of geosynthetic-reinforced soil with a simplified model. Soils and Foundations. 43 (3), 33–42.

Nunez, M.A., Briançon, L., Dias, D., 2013. Analyses of a pile-supported embankment over soft clay: Full-scale experiment, analytical and numerical approaches. Engineering Geology. 153, 53–67.

Parsa-Pajouh, A., Fatahi, B., Khabbaz, H., 2016. Experimental and numerical investigations to evaluate two-dimensional modeling of vertical drain–assisted preloading. International Journal of Geomechanics. 16 (1).

Pasternak, P.L., 1954. On a new method of analysis of an elastic foundation by means of two constants [Gosudarstvennoe Izdatelstvo Literaturi po Stroitelstvu I Arkhitekture]. Moscow: USSR.

Qu, C.Z., 2009. Deformation of geocell with different tensile and compressive modulus. Journal of Geotechnical Engineering.

Rogbeck, Y., Gustavsson, S., Södergren, I., Lindquist, D., 1998. Reinforced piled embankments in Sweden e design aspects. In: Proceedings of the Sixth International Conference on Geosynthetics.

Rowe, R.K., Li, A.L., 2005. Geosynthetic-reinforced embankments over soft foundations. Geosynthetics International. 12 (1), 50–85.

Rowe, R.K., Liu, K.W., 2015. Three-dimensional finite element modelling of a full-scale geosynthetic-reinforced, pile-supported embankment. Canadian Geotechnical Journal. 52 (12), 2041–2054.

Russell, D., Pierpoint, N., 1997. An assessment of design methods for piled embankments. Ground Engineering, 39–44.

Shukla, S.K., Yin, J.H., 2003. Time-dependent settlement analysis of a geosynthetic-reinforced soil. Geosynthetics International. 10 (2), 70–76.

Smith, M.E., 2005. Design of bridging layers in geosynthetic-reinforced column-supported embankments. Doctoral Dissertation, Virginia Tech, Blacksburg.

Suksiripattanapong, C., Chinkulkijniwat, A., Horpibulsuk, S., Rujikiatkamjorn, C., Tanhsutthinon, T., 2012. Numerical analysis of bearing reinforcement earth (BRE) wall. Geotextiles and Geomembranes. 32 (1), 28–37.

Svanø, G., Ilstad, T., Eiksund, G., Want, A., 2000. Alternative calculation principle for design of piled embankments with base reinforcement. In: Proceedings of the 4th GIGS Helsinki.

Tan, S.A., Tjahyono, S., Oo, K., 2008. Simplified plane-strain modeling of stone-column reinforced ground. Journal of Geotechnical and Geoenvironmental Engineering. 134 (2), 185–194.

Terzaghi, K., 1943. Theoretical soil mechanics. John Wiley and Sons, New York.

Timoshenko, S.P., 1921. On the correction for shear of the differential equation for transverse vibrations of prismatic bars. Philosophical Magazine and Journal of Science. 41 (245), 744–746.

Van Eekelen, S.J.M., Bezuijen, A., Oung, O., 2003. Arching in piled embankments; experiments and design calculations. In: Proceedings of Foundations: Innovations, Observations, Design and Practice.

Van Eekelen, S.J.M., Bezuijen, A., Van Tol, A.F., 2011. Analysis and modification of the British Standard BS8006 for the design of piled embankments. Geotextiles and Geomembranes. 29 (3), 345–359.

Van Eekelen, S.J.M., Bezuijen, A., Lodder, H.J., Van Tol, A.F., 2012a. Model experiments on piled embankments. Part I. Geotextiles and Geomembranes. 32 (2012), 69–81.

Van Eekelen, S.J.M., Bezuijen, A., Lodder, H.J., Van Tol, A.F., 2012b. Model experiments on piled embankments. Part II. Geotextiles and Geomembranes. 32 (2012), 82–94.

Van Eekelen, S.J.M., Bezuijen, A., Van Tol, A.F., 2013. An analytical model for arching in piled embankments. Geotextiles and Geomembranes. 39, 78–102.

Van Eekelen, S.J.M., Bezuijen, A., Van Tol, A.F., 2015. Validation of analytical models for the design of basal reinforced piled embankments. Geotextiles and Geomembranes. 43 (1), 56–81.

Winkler, E., 1867. Die Lehre von der Elasticitaet und Festigkeit: mit besonderer Rücksicht auf ihre Anwendung in der Technik für polytechnische Schulen. Dominicus.

Yapage, N.N.S., Liyanapathirana, D.S., 2014. A parametric study of geosynthetic-reinforced column-supported embankments. Geosynthetics International. 21 (3), 213–232.

Yin, J.H., 1997a. Modelling geosynthetic-reinforced granular fills over soft soil. Geosynthetics International. 4 (2), 165–185.

Yin, J.H., 1997b. A nonlinear model of geosynthetic-reinforced granular fill over soft soil. Geosynthetics International. 4 (5), 523–537.

Yin, J.H., 2000a. Closed form solution of reinforced Timoshenko beam on elastic foundation. Journal of Engineering Mechanics. 126 (8), 868–874.

Yin, J.H., 2000b. Comparative modeling study of reonforced beam on elastic foundation. Journal of Geotechnical and Geoenvironmental Engineering. 126 (3), 265–271.

Yu, Y., Bathurst, R.J., 2017. Modelling of geosynthetic-reinforced column-supported embankments using 2D full-width model and modified unit cell approach. Geotextiles and Geomembranes. 45 (2), 103–120.

Zaeske, D., 2001. Zur Wirkungsweise von unbewehrten und bewehrten mineralischen Tragschichten über pfahlartigen Gründungselementen. Schriftenreihe Geotechnik, Uni Kassel. Heft 10 (in German).

Zhang, L., Zhao, M., Zou, X., Zhao, H., 2010. Analysis of geocell-reinforced mattress with consideration of horizontal–vertical coupling. Computers and Geotechnics. 37 (6), 748–756.

Zhang, L., Zhao, M., Hu, Y., Zhao, H., Chen, B., 2012a. Semi-analytical solutions for geosynthetic-reinforced and pile-supported embankment. Computers and Geotechnics. 44, 167–175.

Zhang, L., Zhao, M., Shi, C., Zhao, H., 2012b. Nonlinear analysis of a geocell mattress on an elastic–plastic foundation. Computers and Geotechnics. 42, 204–211.

Zhao, L.S., Zhou, W.H., Fatahi, B., Li, X.B., Yuen, K.V., 2016. A dual beam model for geosynthetic-reinforced granular fill on an elastic foundation. Applied Mathematical Modelling. 40 (21–22), 9254–9268.

Notation

The following symbols are used in this paper:

A_c: plan area of the column (m^2);

A_h: cross section area of the granular layer in hogging region after cracking (m^2);

A_s: cross section area of the granular layer in sagging region after cracking (m^2);

A_r: cross section area of the geosynthetic reinforcement (m^2);

a_r: area replacement ratio (non-dimensional);

C: shear stiffness of the beam (kN/m);

D_h: equivalent bending stiffness of the load transfer platform in hogging region (kN.m);

D_s: equivalent bending stiffness of the load transfer platform in sagging region (kN.m);

d: diameter of the column (m);

E_c: Young's modulus of the controlled modulus column material (kPa);

E_g: Young's modulus of the granular material in load transfer platform (kPa);

E_r: elastic stiffness of the geosynthetic reinforcement (kPa);

G: shear modulus of the soft soil (kPa);

H: depth of the soft soil (m);

h: thickness of the load transfer platform before cracking (m);

h_h: distance of the neutral axis from the compression surface of the load transfer platform for hogging moment (m);

h_s: distance of the neutral axis from the compression surface of the load transfer platform for sagging moment (m);

I_h: second moment of inertia of the granular fill about neutral axis for hogging (m^3);

I_s: second moment of inertia of the granular fill about neutral axis for sagging (m^3);

M: bending moment o (kN.m);

n: modular ratio (non-dimensional);

$(K_c)_{eq}$: equivalent modulus of the subgrade reaction for column (kN/m);

k_c: modulus of subgrade reaction for the column (kN/m^2/m);

k_l: modulus of subgrade reaction for the soft soil foundation attached to the bottom of shear layer (kN/m^2/m);

k_{sc}: shear correction coefficient of the Timoshenko beam (non-dimensional);

k_u: modulus of subgrade reaction for the soft soil foundation attached to LTP (kN/m^2/m);

p: transverse pressure on the beam from super structure (kPa);

q: normal stress at the interface of the beam and the soft soil (kPa);

S: centre to centre spacing between the two adjacent columns (m);

s: clear spacing between the two adjacent columns (m);

S_r: tensile stiffness of the geosynthetic (kN/m);

S_r^b: tensile stiffness of the bottom geosynthetic reinforcement (kN/m);

S_r^t: tensile stiffness of the top geosynthetic reinforcement (kN/m);

T: tension mobilised in the geosynthetic layer (kN/m);

V: shear force (kN/m);

w: transverse deflection (m);

y_h: distance between the neutral axis and the centroid axis of the load transfer platform in hogging region (m);

y_s : distance between neutral and centroid axes of the load transfer platform in sagging region (m);

y_r^b: distance of the bottom geosynthetic layer from the centroid axis of load transfer platform (m);

y_r^t : distance of the top geosynthetic layer from the centroid axis of load transfer platform (m);

υ_g : Poisson's ratio of the granular material (non-dimensional);

υ_r: Poisson's ratio of the geosynthetic reinforcement (non-dimensional);

υ_r^t : Poisson's ratio of the top geosynthetic reinforcement (non-dimensional);

υ_r^b: Poisson's ratio of the bottom geosynthetic reinforcement (non-dimensional);

θ: rotation angle of the cross section (radian).

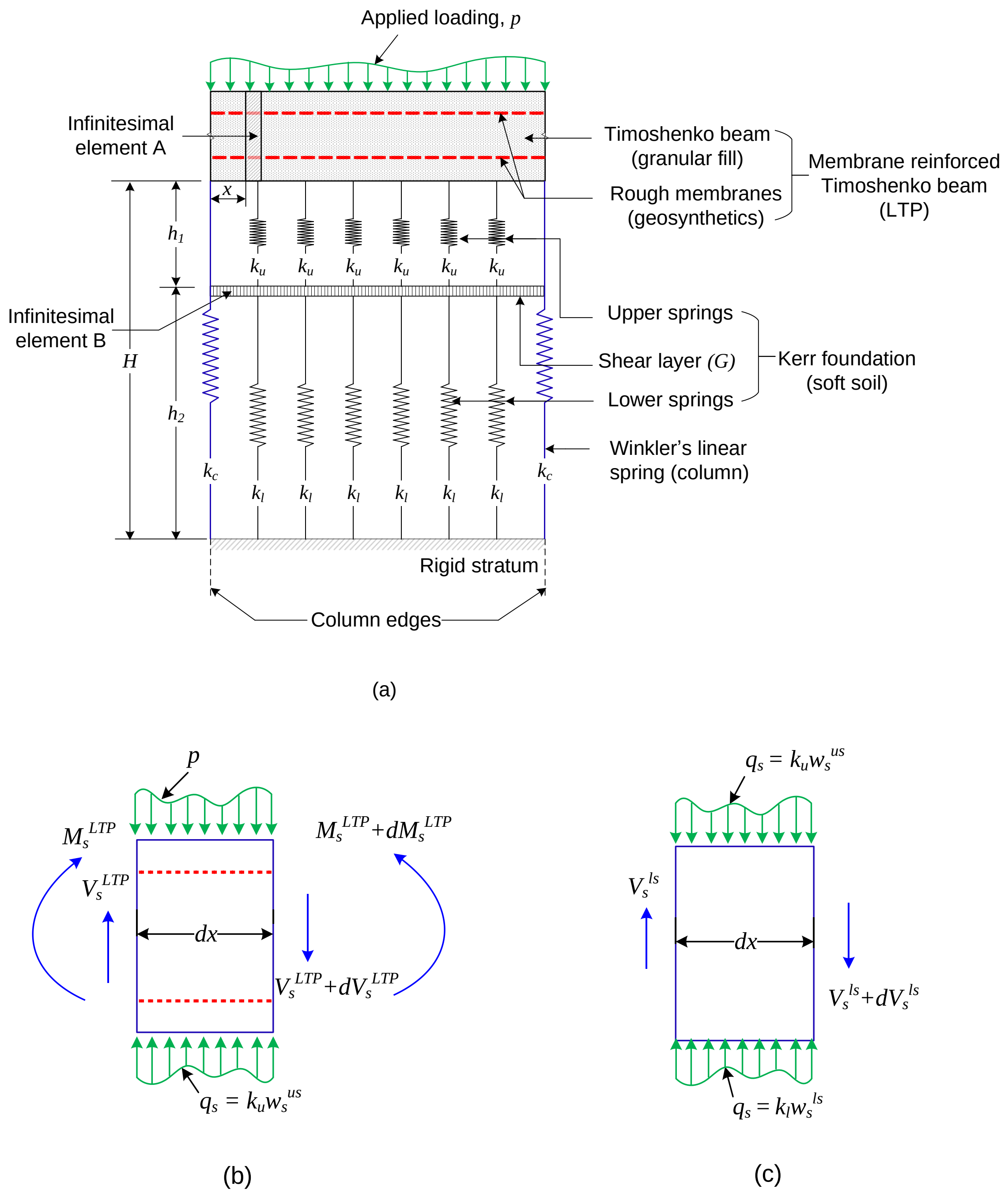

Fig. 1. Illustration of (a) proposed mechanical model of load transfer platform on column improved soft soil in plane strain condition, (b) free-body diagram of element A in sagging part, and (c) free-body diagram of element B in sagging part.

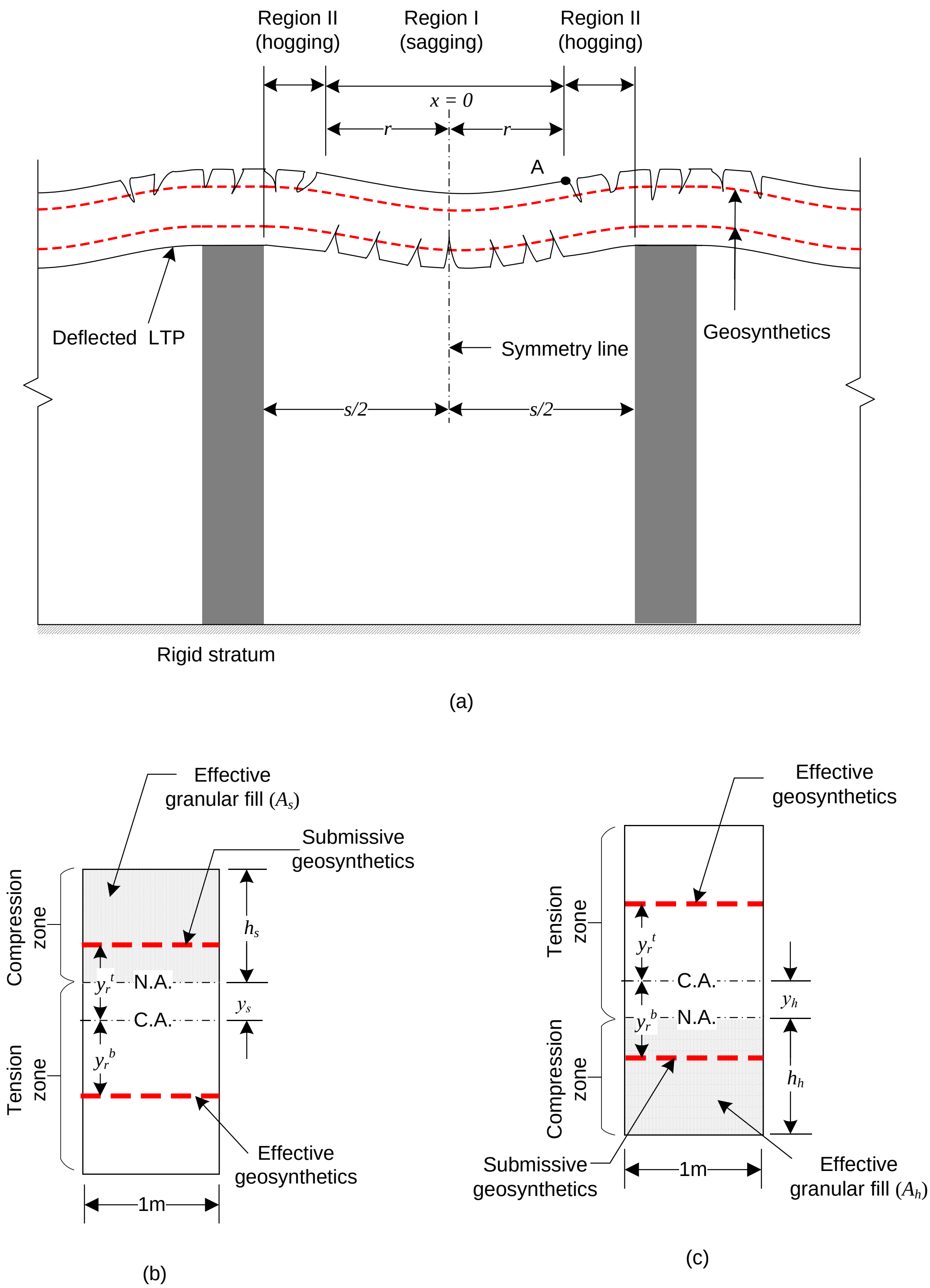

Fig. 2. Typical diagram of (a) deflection profile of load transfer platform (LTP), (b) effective cross-section of LTP in sagging region, and (c) effective cross-section of LTP in hogging region.

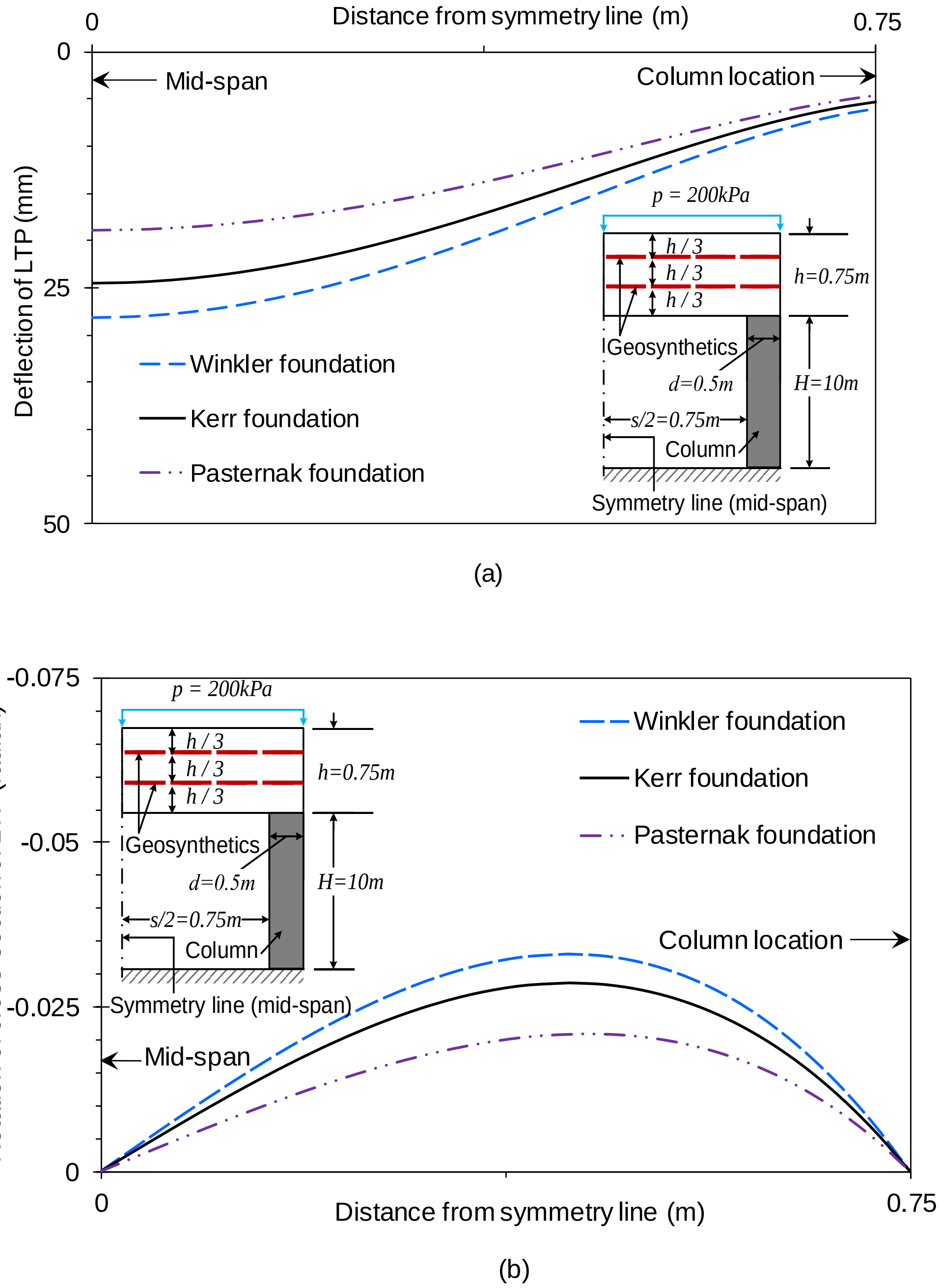

Fig. 3. Comparison of (a) settlement and (b) rotation profiles of LTP considering soft soil as Kerr, Pasternak, and Winkler foundation models.

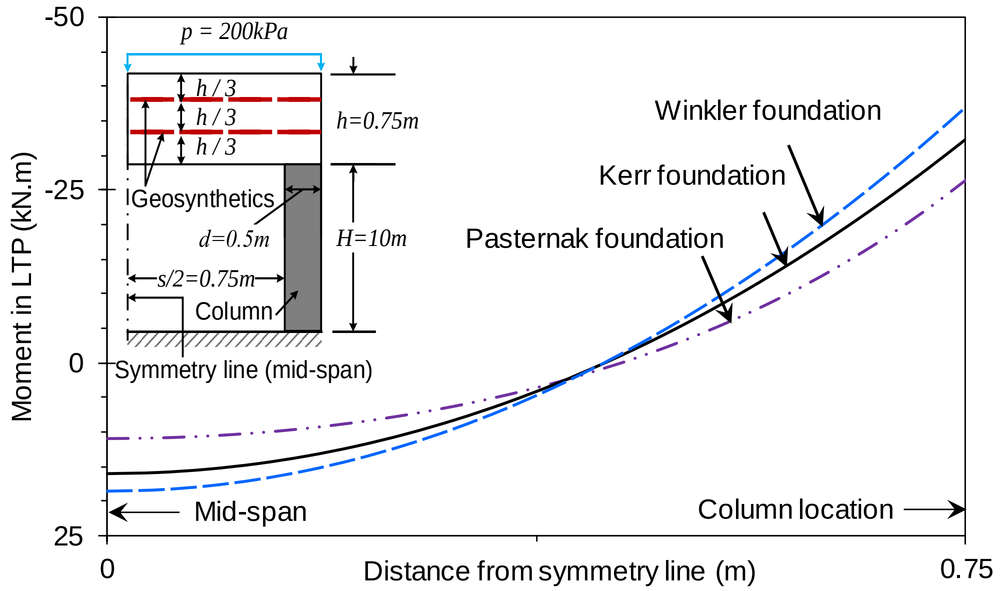

-50
-25
0
25
Moment in LTP (kN.m)
p = 200kPa
h / 3
h / 3
h / 3
h=0.75m
Geosynthetics
d=0.5m
H=10m
s/2=0.75m
Column
Symmetry line (mid-span)
Winkler foundation
Kerr foundation
Pasternak foundation
Mid-span
Column location
0
Distance from symmetry line (m)
0.75

(a)

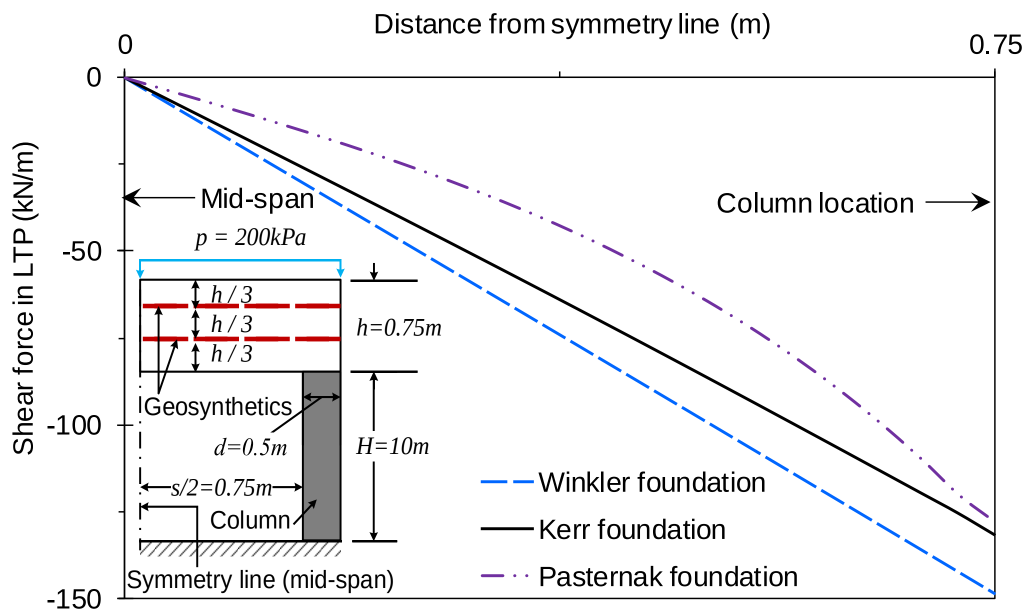

Distance from symmetry line (m)
0
0.75
0
-50
-100
-150
Shear force in LTP (kN/m)
Mid-span
Column location
p = 200kPa
h / 3
h / 3
h / 3
h=0.75m
Geosynthetics
d=0.5m
H=10m
s/2=0.75m
Column
Symmetry line (mid-span)
Winkler foundation
Kerr foundation
Pasternak foundation

(b)

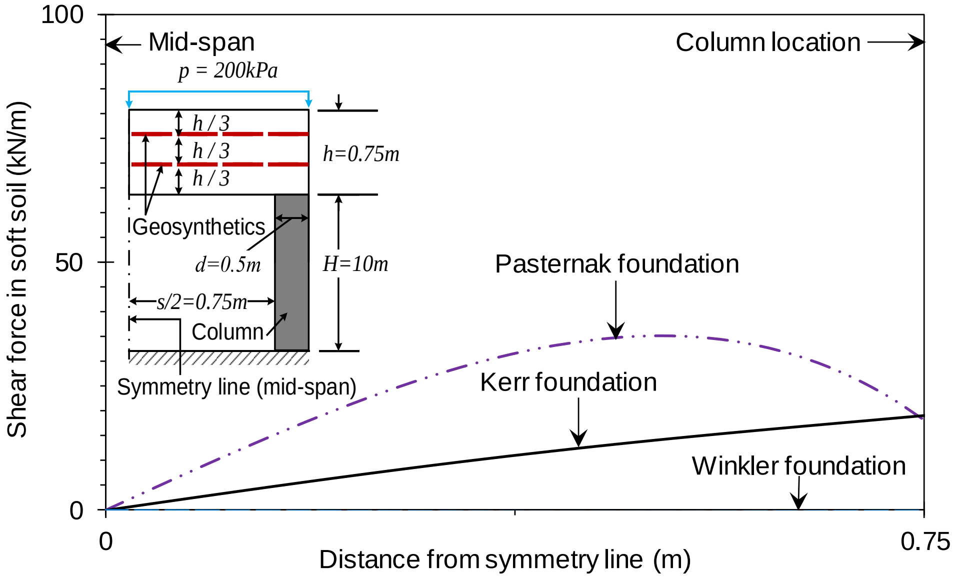

(c)

Fig. 4. Comparison of (a) bending moment of LTP, (b) shear force in LTP, and (c) shear force developed in soft soil considering soft soil as Kerr, Pasternak, and Winkler foundation models

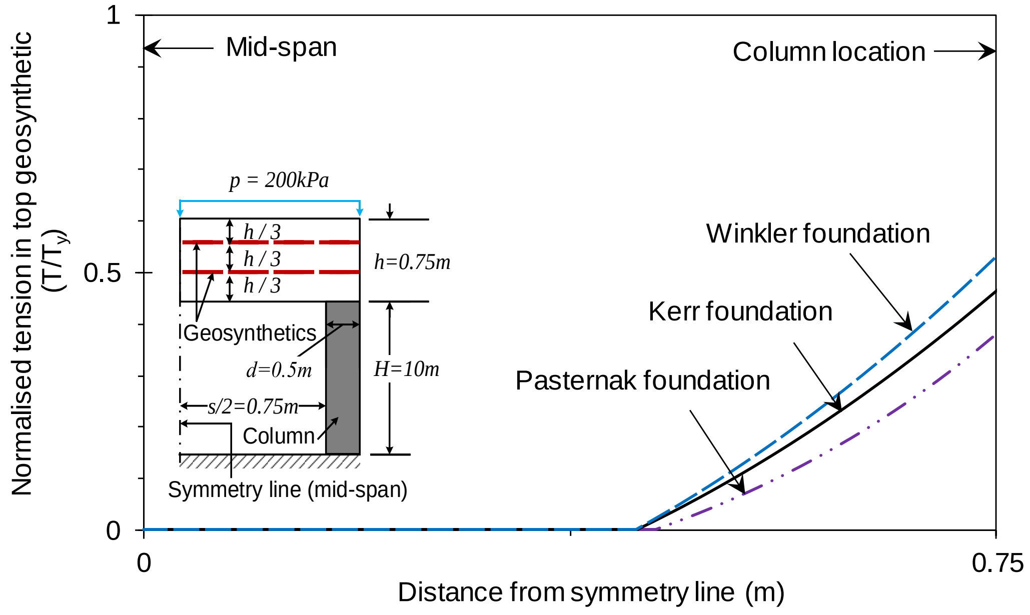

(a)

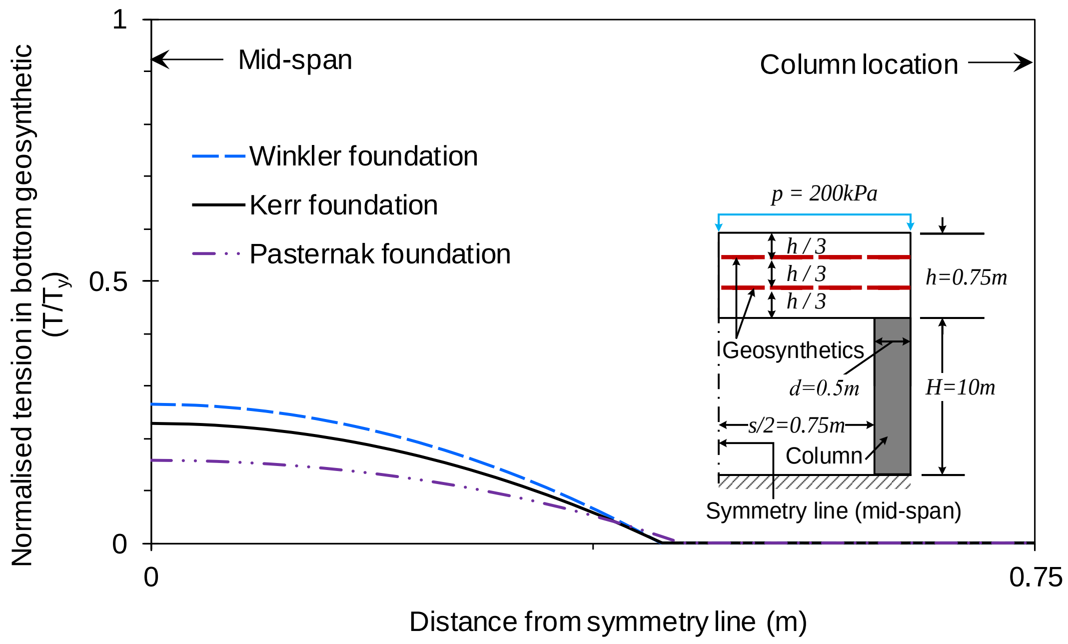

(b)

Fig. 5. Comparison of mobilised tensions in (a) top and (b) bottom geosynthetic layers considering soft soil as Kerr, Pasternak, and Winkler foundation models.

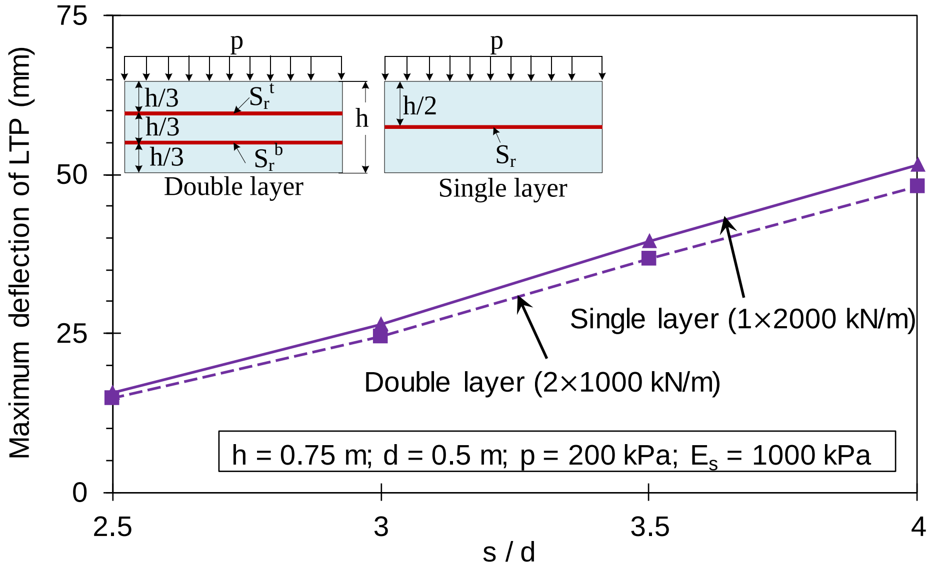

(a)

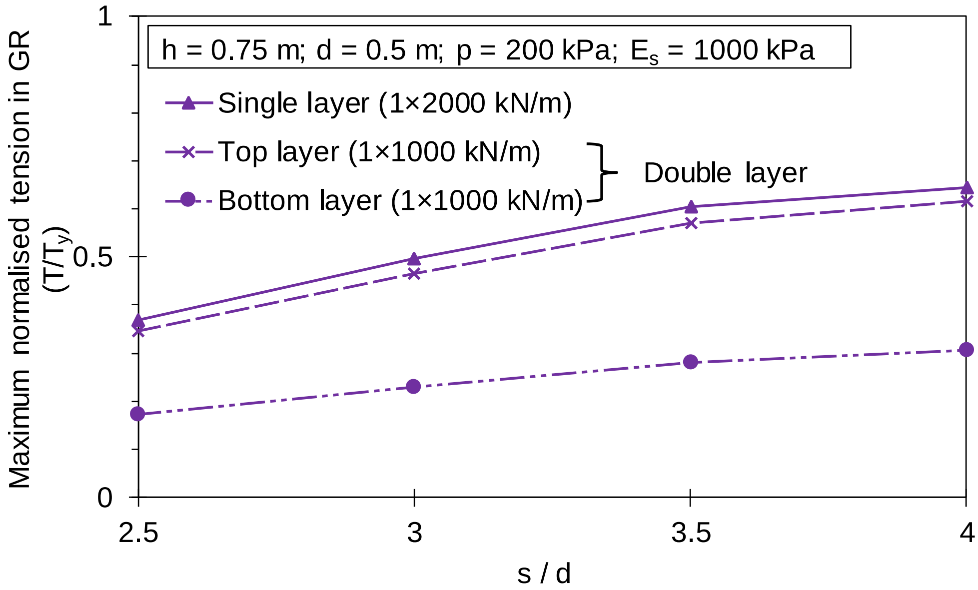

(b)

Fig. 6. Effect of column spacings for the case of LTP on Kerr foundation model on (a) the maximum deflections of LTP and (b) the maximum normalised tensions in the geosynthetics.

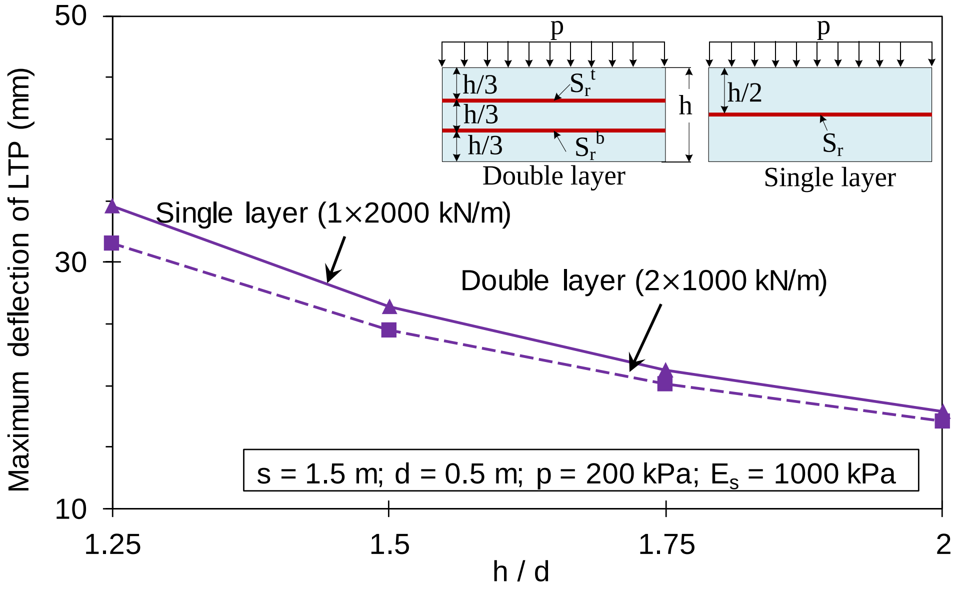

(a)

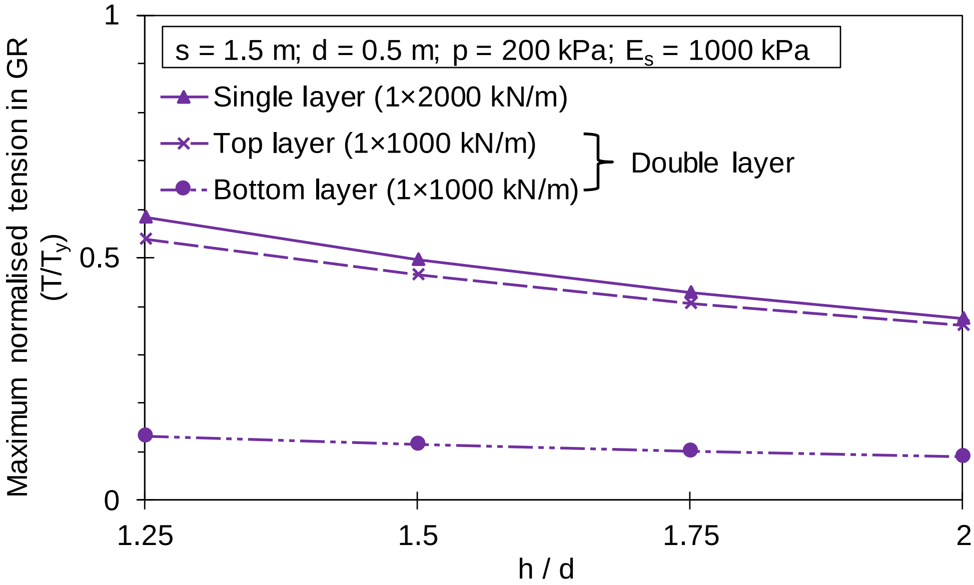

(b)

Fig. 7. Effect of LTP thicknesses for the case of LTP on Kerr foundation model on (a) the maximum deflections of LTP and (b) the maximum normalised tensions in the geosynthetics.

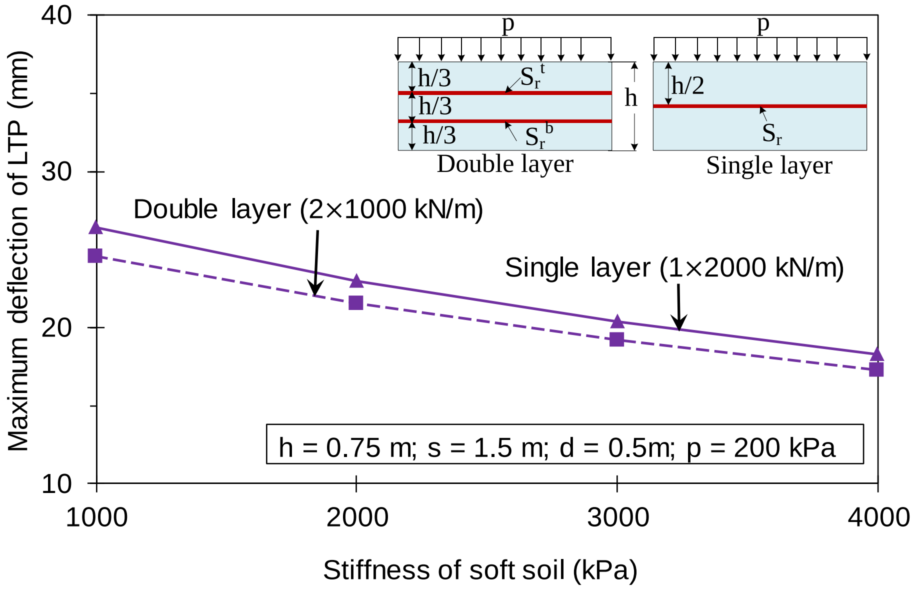

(a)

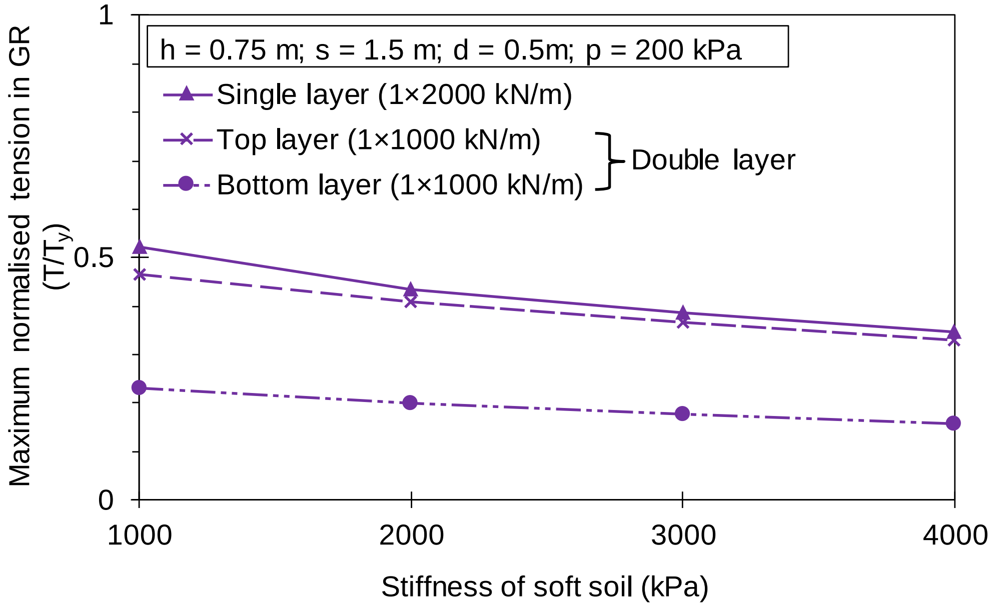

(b)

Fig. 8. Effect of soft soil stiffnesses for the case of LTP on Kerr foundation model on (a) the maximum deflections of LTP and (b) the maximum normalised tensions in the geosynthetics.

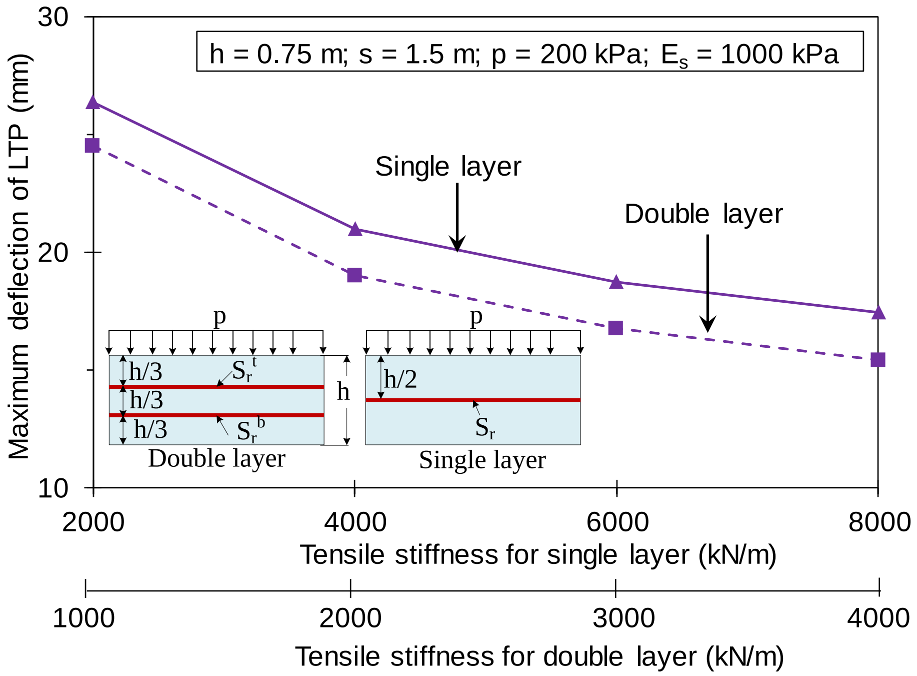

(a)

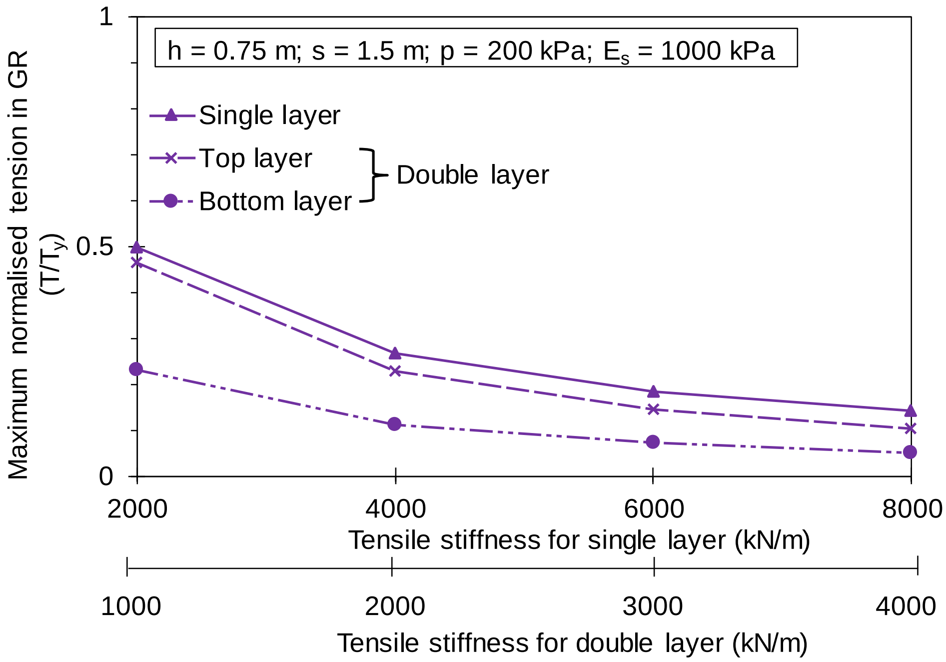

(b)

Fig. 9. Effect of tensile stiffnesses of geosynthetic reinforcement for the case of LTP on Kerr foundation model (a) the maximum deflections of LTP and (b) the maximum normalised tensions in the geosynthetics.

Table 1

Material properties used in the baseline analysis.

Material	Parameters	
Soft clay	Stiffness (E_s) = 1000 kPa , Poisson's ratio (ν_s) = 0.3	
CMC	Stiffness (E_c) = 10,000 MPa , Poisson's ratio (ν_c) = 0.25	
Geosynthetics	Multilayer	Tensile stiffness (S_r^t = S_r^b) = 1000 kN/m, Poisson's ratio (ν_r^t = ν_r^b) = 0.3
	Single layer	Tensile stiffness (S_r) = 2000 kN/m, Poisson's ratio (ν_r) = 0.3
Granular fill	Stiffness (E_g) = 35 MPa, Poisson's ratio (ν_g) = 0.3	

Table 2

Adopted range of parameters used in the parametric study.

Influencing factor	Range of value
Stiffness of soft soil, E_s (kPa)	1000*, 2000, 3000, 4000
Centre to centre spacing of columns, S (m)	1.75, 2.0*, 2.25, 2.5
	S_r^t: 1000*, 2000, 3000, 4000
Tensile stiffness of geosynthetics, (kN/m)	S_r^b : 1000*, 2000, 3000, 4000
	S_r: 2000*, 4000, 6000, 8000
Thickness of granular layer, h (m)	0.625, 0.75*, 0.875, 1
Loading, p (kPa)	125, 150, 175, 200*

* Parameters used for baseline analysis.

Table 3

Calculated properties and geometries of reinforced granular layer for baseline case.

Parameters	Double layer	Single layer
h_s (m)	0.14	0.16
h_h (m)	0.14	0.16
y_s (m)	0.23	0.22
y_h (m)	0.23	0.22
D_s (kN.m)	161	140
D_h (kN.m)	161	140
C (kN/m)	9.2×10^3	9.2×10^3

List of Figures

Fig. 1. Illustration of (a) proposed mechanical model of load transfer platform on column improved soft soil in plane strain condition, (b) free-body diagram of element A in sagging part, and (c) free-body diagram of element B in sagging part.

Fig. 2. Typical diagram of (a) deflection profile of load transfer platform (LTP), (b) effective cross-section of LTP in sagging region, and (c) effective cross-section of LTP in hogging region.

Fig. 3. Comparison of (a) settlement and (b) rotation profiles of LTP considering soft soil as Kerr, Pasternak, and Winkler foundation models.

Fig. 4. Comparison of (a) bending moment of LTP, (b) shear force in LTP, and (c) shear force developed in soft soil considering soft soil as Kerr, Pasternak, and Winkler foundation models

Fig. 5. Comparison of mobilised tensions in (a) top and (b) bottom geosynthetic layers considering soft soil as Kerr, Pasternak, and Winkler foundation models.

Fig. 6. Effect of column spacings for the case of LTP on Kerr foundation model on (a) the maximum deflections of LTP and (b) the maximum normalised tensions in the geosynthetics.

Fig. 7. Effect of LTP thicknesses for the case of LTP on Kerr foundation model on (a) the maximum deflections of LTP and (b) the maximum normalised tensions in the geosynthetics.

Fig. 8. Effect of soft soil stiffnesses for the case of LTP on Kerr foundation model on (a) the maximum deflections of LTP and (b) the maximum normalised tensions in the geosynthetics.

Fig. 9. Effect of tensile stiffnesses of geosynthetic reinforcement for the case of LTP on Kerr foundation model (a) the maximum deflections of LTP and (b) the maximum normalised tensions in the geosynthetics.

List of Tables

Table 1 Material properties used in the baseline analysis.

Table 2 Adopted range of parameters used in the parametric study.

Table 3 Calculated properties and geometries of reinforced granular layer for base line case.